# AEROSOL FORMATION IN $CO_2$ CAPTURE PLANTS – ASPEN PLUS SIMULATION MODEL

**Nursultan Galymzhanov**, BEng Energy Engineering

**Submitted in fulfilment of the requirements**
**for the degree of Masters of Science**
**in Chemical Engineering**


**School of Engineering**
**Department of Chemical Engineering**
**Nazarbayev University**

53 Kabanbay Batyr Avenue,
Astana, Kazakhstan, 010000

**Supervisors:** Dr. Mehdi Torkmahalleh
Dr. Dhawal Shah

**December, 2017**

# Declaration

I hereby, declare that this manuscript, entitled “Aerosol Formation in $CO_2$ Capture Plants – Aspen Plus Simulation Model”, is the result of my own work except for quotations and citations which have been duly acknowledged.

I also declare that, to the best of my knowledge and belief, it has not been previously or concurrently submitted, in whole or in part, for any other degree or diploma at Nazarbayev University or any other national or international institution.

Nursultan Galymzhanov

26/01/2018

# Abstract

One of the most promising technologies available for decreasing $CO_2$ concentration in the atmosphere is Post Combustion $CO_2$ Capture (PCCC). The process is based on absorption-desorption of carbon dioxide by a solvent. Amine based aqueous solutions are considered as the state of the art solvent for PCCC. However, its use is associated with MEA emissions from an absorber column through vapour and aerosol phases. Aerosol emission has only recently been detected, and reported to be related to the degree of supersaturation of gas.

The objective of this study was to develop a new conceptual model to estimate heat and mass transfer rates between gas and particulate phases using Aspen Plus simulation software. Also, validation of the model was performed by comparing it with results of an experimental mini-plant developed by TNO group in Netherlands.

In the model presented in this study, interaction between the gas and the solvent, and the gas and the particles was split by modelling the gas-solvent interaction in the absorber and the gas-particles interaction in separate absorber columns representing sections of a discretised absorber. A method was presented to estimate particle formation due to nucleation and to correct the MEA loss predicted by Aspen Plus.

The $CO_2$ removal efficiency was estimated to be 95%. The estimated total molecular mass transfer rate from the gas phase at the top of the absorber column to

the particle phase was found to be $-7.3\times10^{-10}$ kg/s, indicating net molecular mass transfer from the particle to the gas phase. The mass transfer due to nucleation was estimated to be $1.92487\times10^{-6}$ kg/s. The amount of particle phase MEA emission was found to depend on the temperature inside the absorber, temperature bulge, gas supersaturation ratio, volume of particles entering the absorber and $H_2SO_4$ concentration in the entering gas. The particle phase MEA emission due to the molecular mass transfer from the gas phase to the particle phase was found to be 0.3 $mg/Nm^3_{gas}$, while particle phase MEA emission resulted from the nucleation mass transfer was 697.0 $mg/Nm^3_{gas}$. Thus, the total particle MEA emission was estimated to be 697.3 $mg/Nm^3_{gas}$. The estimated nucleation rate is approximately $2\times10^{15}$ $particles.cm^{-3}.s^{-1}$. Gas phase MEA emission was found to be 1.3 $mg/Nm^3_{gas}$.

# Acknowledgements

I express my gratitude to my supervisor Dr. Mehdi Torkmahalleh and to my co-supervisor Dr. Dhawal Shah. Their supervision and direction has allowed me to complete this study. I am thankful to them for the knowledge they provided to me.

I thank Nazarbayev University and its staff for providing me the opportunity to study Chemical Engineering and receive master's degree.

I express my gratitude to my colleagues who shared this great journey with me.

Finally, I thank my family who always supported and encouraged me in all of my pursuits.

# Table of Contents

# List of Tables

# List of Figures

# Chapter 1 - Introduction

It is commonly known that nowadays human being utilises enormous amounts of fossil fuels. Fossil fuels used today include oil and its products, coal, natural and petroleum gas. The consensus, that is globally accepted and proven scientifically, is that human activities lead to significant increase in $CO_2$ concentration in the atmosphere by combustion of fossil fuels. The increase in $CO_2$ concentration results in the global climate change observed over the past few decades. (Parliament of Australia, 2010)

One of the most promising technologies, aiming to decrease global $CO_2$ emissions, is Post Combustion $CO_2$ Capture (PCCC) (Abu Zahra, 2007). It is a well-understood and the most mature technology for preventing $CO_2$ emissions (Rochelle, 2009). The basic technology for $CO_2$ capture and storage was patented in 1930 (Rochelle, 2009). The process is based on absorption-desorption of carbon dioxide by a solvent. In an absorber column the solvent flows from the top and the gas flows from the bottom. Reaction between the two flows is exothermic, and results in transfer of $CO_2$ from the gas to the solvent. Desorption is a reverse process taking place in a stripper. $CO_2$ is removed from the solvent by supplying the stripping column with additional heat.

The state of the art solvents for PCCC are amine based aqueous solutions (Rao and Rubin, 2002; Alie et al., 2005). Their advantages include high reactivity, low cost and high absorbing capacity (IEA CCC, 2007). However, one of the major problems, associated with $CO_2$ capture, is loss of solvent due to emissions, thermal degradation and oxidative degradation (Khakharia et al., 2014a). Solvent losses due to emissions subdivide into three categories: (1) vapour emissions (due to component's volatility); (2) carryover as a result of mechanical entrainment; and (3) aerosol emissions (emissions due to particulate matter) (Khakharia et al., 2015). The first two types of emissions are well understood. They are effectively reduced by a water wash at the top of the absorber. However, the water wash is ineffective in catching aerosol emissions due to their submicron size. (da Silva et al., 2013; Gretscher and Schaber, 1999)

Schaber (1994) defines aerosols as "suspensions of particles and gases which can be considered as stable systems in a gravitational field within a certain space of time". According to Gretscher and Schaber (1999), the mechanism of particle formation and growth is related to the degree of supersaturation. When supersaturation is high, then nucleation takes place. Nuclei can be formed by molecules of condensing components (homogeneous nucleation), and/or on the impurities in the flue gas (heterogeneous nucleation) (Gretscher and Schaber, 1999).

Aerosol emission from the carbon capture process is not yet well studied and clearly understood by researchers. Available information is very limited. Therefore, validation of a new study is frequently difficult.

The objective of this study was to develop a new conceptual model to estimate heat and mass transfer rates between gas and particulate phases using Aspen Plus simulation software. The new model gives opportunity to study particle emission exiting from the absorber column, i.e. its composition and flowrate, and factors that have influence on it. Also, validation of the model was performed by comparing it with results of an experimental mini-plant developed by TNO group in Netherlands.

# Chapter 2 - Literature review

Prediction of vapour based MEA emission from PCCC plants is easy and straightforward task that has been extensively studied by researchers (Mertens et al., 2012; Nguyen et al., 2010; Trollebø et al., 2013, Khakharia et al., 2014b). On the other hand, number of experimental and simulation studies published on PM emissions understanding is very limited. This chapter presents a literature review that was performed to understand what studies have been conducted in the area of PM emissions from PCCC plants.

## 2.1. Experiments

Khakharia et al., (2013) performed an investigation of aerosol based emissions of MEA due to sulphuric acid aerosol and soot in a typical Post Combustion $CO_2$ capture process.

***Figure 2.1.1: Schematic representation of the pilot plant for sulphuric acid aerosol generation (Khakharia et al., 2013)***

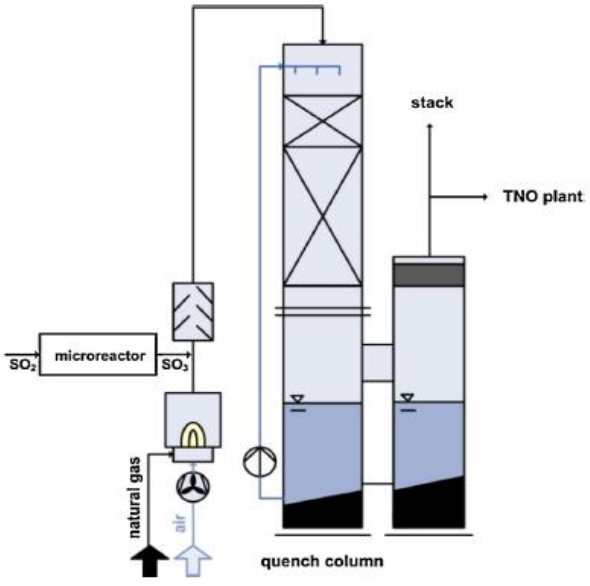

Flue gas containing particulate nuclei was generated in the pilot plant at the Karlsruhe Institute of Technology, Germany. The schematic of the pilot plant is shown in Figure 2.1.1. The particle concentration in this pilot plant could be varied between $10^4$ and $10^6$ per $cm^3$. $SO_3$ was added to the flue gas where it completely converted to $H_2SO_4$ by reacting with water vapour from combustion. The flue gas was sent to a quench cooler where it was rapidly cooled, resulting in aerosol generation with number concentration in the order of $10^8$ and size well below 100 nm.

$CO_2$ capture mini-plant was run at TNO, Netherlands. The absorber was 3.5 m high and 4.5 cm diameter packed with Sulzer Mellapak 2X. It had no water wash or demister. Additional $CO_2$ was added to the flue gas entering the mini-plant to obtain $CO_2$ concentrations in the range 0.7-13 vol.%.

To analyse the gas phase, a Fourier Transform InfraRed analyser GASMET CX 4000 was used. The work of the FTIR analyser is based on the measurement of a large wavelength band in the infrared region and calculating the concentration of each component by using inverse optimisation technique.

A baseline study was conducted to observe the emissions in the absence of soot and sulphuric acid. The MEA emission was found to be 45 $mg/Nm^3$. In addition, the temperature profile in the absorber was created. The temperature increased from the bottom to approximately two-thirds of the column because of the exothermic

reaction between MEA and $CO_2$. Then, in the upper zone of the column, the temperature decreased because of heat transfer to the cold solvent entering from the top.

At low soot concentration ($10^4$ per $cm^3$), MEA emission increased to 100 $mg/Nm^3$. At high soot concentration ($10^6$ per $cm^3$), MEA emission reached 200 $mg/Nm^3$. It was found that this behaviour was instantaneous and reversible. The reason for the MEA emission increase was that as the soot number concentration increased, more surface area was provided for MEA transfer to the soot.

Three levels of $H_2SO_4$ aerosol concentration were tested: 1.02, 1.18 and $1.42\times10^8$ per $cm^3$ indicated as low, medium and high, respectively. It was found that MEA emissions directly depend on $H_2SO_4$ concentration in the flue gas. At high $H_2SO_4$ concentrations, MEA emission can reach 600-1200 $mg/Nm^3$. The effect was found to be instantaneous. The reason for the increase in MEA emission is same as in the case of soot.

Soot particle concentration was varied between $10^4$ and $10^6$ per $cm^3$, and $H_2SO_4$ particle concentration in the range of $10^8$ per $cm^3$ to observe their simultaneous effect on MEA emission. It was found that effect of soot particle concentration on MEA emission was higher than that of $H_2SO_4$ particle concentration.

$CO_2$ content in the flue gas variation from 0.7 vol.% to 12.1 vol.% was found to have instantaneous and reversible effect on MEA emission. MEA emission increased from 220 mg/$Nm^3$ to 1600-1800 mg/$Nm^3$ in seconds. When the $CO_2$ content is increased, more heat is released during MEA-$CO_2$ reaction resulting in a higher temperature bulge. Temperature bulge is defined as the difference between the gas temperature at the hottest and the top zones of the absorber.

Mertens et al. (2014) study was performed to present data on the particle size distribution, and number entering and leaving the absorber. This work was the first to present this kind of data.

Pilot plants used for $H_2SO_4$ generation and carbon capture, as well as an FTIR analyser, were all same as used in Khakharia et al. (2013).

The main measurement instrument in this work was the electrical low pressure impactor ELPI$^+$. In this device the particles were charged by corona charging and subsequently separated in a low pressure cascade impactor with 14 electrically insulated collection stages. The measured current signals were proportional to the number concentration and size.

The work results were compared to the work conducted by Brachert et al. (2014). The experimental set-ups for $H_2SO_4$ aerosol generation in two works were similar to each other. However, Mertens et al. (2014) used a fan to blow the flue gas

into the absorber, whereas Brachert et al. (2014) installed a vacuum pump behind the absorber.

Particle sizes in front of the absorber measured by Brachert et al. (2014) were larger than that of Mertens et al. (2014) because the particles shrinked as they passed through a fan before entering the absorber. As a result, the number concentration of particles increased from $2.1\times10^8$ to $6.5\times10^8$ per $cm^3$. Similarly to Brachert et al. (2014), it was confirmed that particle sizes entering the absorber were well below 200 nm.

It was found by comparing measured size distribution of particles entering the absorber and leaving it that they grew inside the absorber. The largest size measured before the absorber was approximately 0.3 μm. In contrast, the largest particle size leaving the absorber was around 10 μm. This was due to the uptake of MEA and water by particles.

The number concentration decreased from $6.5\times10^8$ to $1.3\times10^8$ per $cm^3$ because of larger particles and coagulation.

MEA emissions in the order of 3000-3500 $mg/Nm^3$ were measured at the outlet of the absorber. To compare, MEA emissions in the absence of $H_2SO_4$ aerosol were 45 $mg/Nm^3$.

Theoretical calculation was performed to evaluate whether the measured particle sizes and numbers can contain 3000 $mg/Nm^3$ of MEA emissions.

Kolderup et al. (2012) reported 15 wt.% MEA concentration in the flue gas leaving an absorber column. To contain 3000 mg/$Nm^3$ of MEA, the flue gas must contain 20 ml of water per $Nm^3$.

By assuming that particles were 100% water, the volume of water the particles contain based on their size and number concentration was calculated. The plot of ml of water in particle against particle size was plotted for different particle concentrations. For number concentrations between $1\times10^7$ and $1\times10^8$ per $cm^3$ and 20 ml water per $Nm^3$, the particle size should be 1 μm. However, the actual size of particles is less than 0.1 μm and contain very small amounts of water due to their submicron size. At 0.1 μm particle size and a ten times dilution, the water content was found to be 2.5 ml/$Nm^3$. It was concluded that decreasing the dilution to zero can result in increasing the water content by one order of magnitude. Also, assumption of 15 wt.% MEA in the flue gas can be not accurate.

In the study performed by Khakharia et al. (2015) variation of the following parameters in a $CO_2$ capture mini-plant on particle formation was tested: lean solvent temperature, pH of the lean solvent, and $CO_2$ concentration in the flue gas. Also, other commonly used solvents such as mixtures of AMP with Pz, and AMP with potassium taurate (Ktau) were evaluated for the potential of particle formation.

Pilot plants used for $H_2SO_4$ generation and carbon capture, as well as an FTIR analyser, were all same as described in Khakharia et al. (2013). The number

concentration of particles was measured by a condensation particle counter (CPC; PALAS UFCPC with sensor 200).

Increasing the lean solvent temperature from 40°C to 80°C by increments of 10°C, and maintaining all other input parameters unchanged resulted in an increase in the temperature along the column, especially in the upper part. The temperature bulge (temperature difference between the hottest zone and the top zone) reduced at higher lean solvent temperatures. The water content increased from 10 vol.% to 28 vol.%. Increasing the lean solvent temperature from 40°C to 50°C resulted in the decrease in MEA emissions, which were aerosol based, from 1900 mg/Nm$^3$ to 1600 mg/Nm$^3$. At the lean solvent temperature of 60°C emissions were 1200 mg/Nm$^3$. Further increase in the lean solvent temperature decreased emissions less because vapour emissions of MEA started to increase.

When AMP-Pz (next generation $CO_2$ capture solvent) was used as the solvent, the temperature in the absorber was lower, and the temperature bulge moved to the bottom of the column. The emissions of AMP and Pz directly and instantaneously followed the trend of particle number concentration. When the $H_2SO_4$ particle concentration increased from $9.7\times10^7$ to $1.4\times10^8$ per cm$^3$, emissions of AMP increased from 2146 mg/Nm$^3$ to 2940 mg/Nm$^3$. Emissions of Pz increased from 312 mg/Nm$^3$ to 416 mg/Nm$^3$. In the case of absence of $H_2SO_4$ particles, the emissions were 393 mg/Nm$^3$ and 15 mg/Nm$^3$ respectively.

The lean solvent pH depends on how much $CO_2$ is stripped in the stripper and, thus, on the stripper operating temperature. The more $CO_2$ is stripped, the higher the lean solvent pH is. It was found that as the pH of the lean solvent increased, so did the AMP and Pz emissions. This increase occurred because more $CO_2$ reacted with MEA resulting in a higher temperature profile. The maximum pH of 11 resulted in maximum AMP and Pz emissions, 2249 mg/$Nm^3$ and 350 mg/$Nm^3$ respectively.

When variation of the $CO_2$ content in the flue gas from 12.7 vol.% to 0.7 vol.% was tested with AMP-Pz as a solvent, the temperature inside the absorber decreased with the decrease in the $CO_2$ content as less $CO_2$ participated in the exothermic reaction with the solvent. The emission of AMP and Pz increased as the $CO_2$ content was decreased from 12.7 vol.% to 6 vol.% and reached 2200 mg/$Nm^3$ and 226 mg/$Nm^3$ respectively. During the further decrease in $CO_2$ content up to 0.7 vol.%, the emission of AMP and Pz reduced.

Solvent made of AMP and Ktau was tested to understand whether aerosol emissions occur when a non-volatile amino acid salt was present. The maximum temperature was observed in the bottom of the column in this case. It was found that AMP emissions were approximately same in presence and absence of $H_2SO_4$ particles. It means that AMP is not present in the particle phase, but only in the gas phase.

The authors stated that the three main parameters, that aerosol based emissions depend on, are particle number concentration, supersaturation and reactivity of amine.

A means of understanding the dynamics of aerosol fields in gas-liquid contacting devices by developing an *in situ* particle analysis technique called Phase Doppler Interferometry (PDI) was presented in the work by Fulk et al. (2017). Particle size distributions (PSD) and total particle densities were measured and compared to FTIR data on bench and pilot scale apparatuses for two amine systems: Pz and MEA.

A portable, weatherproof, simultaneous sampling system for FTIR and PDI was designed and constructed for testing at different pilot plants. A large slipstream was withdrawn from a process duct through a blower. A small fraction of the slipstream was drawn into DX4000 portable FTIR analyser. The rest of the slipstream was passed through the PDI analyser.

The sampling locations were at the Pickle Research Campus (PRC) pilot plant at the University of Texas at Austin, USA and at the Slipstream Solvent Test Unit (SSTU) pilot plant of the National Carbon Capture Centre (NCCC) in Alabama, USA.

PDI and FTIR sampling was performed at NCCC over a period of seven days. The PDI measured total particle densities up to $10^7$ particles per $cm^3$, mostly of micron range. The average fitting error between the PDI and FTIR was 40%.

Correlation between average diameter and total particle density for the two blower locations showed that the average diameter decreased with the total particle density due to the mass balance of condensable material. The more condensation sites, that occur at higher particle densities, the less growth can a single particle achieve.

In the study by Fujita et al. (2017), Toshiba performed evaluation of amine emissions from 10 ton-$CO_2$/day scale pilot plant within 30 wt.% MEA solution and Toshiba solvent (TS-1).

***Figure 2.1.2: Schematic of PCC Pilot Plant and Testing apparatus (Fujita et al. 2017)***

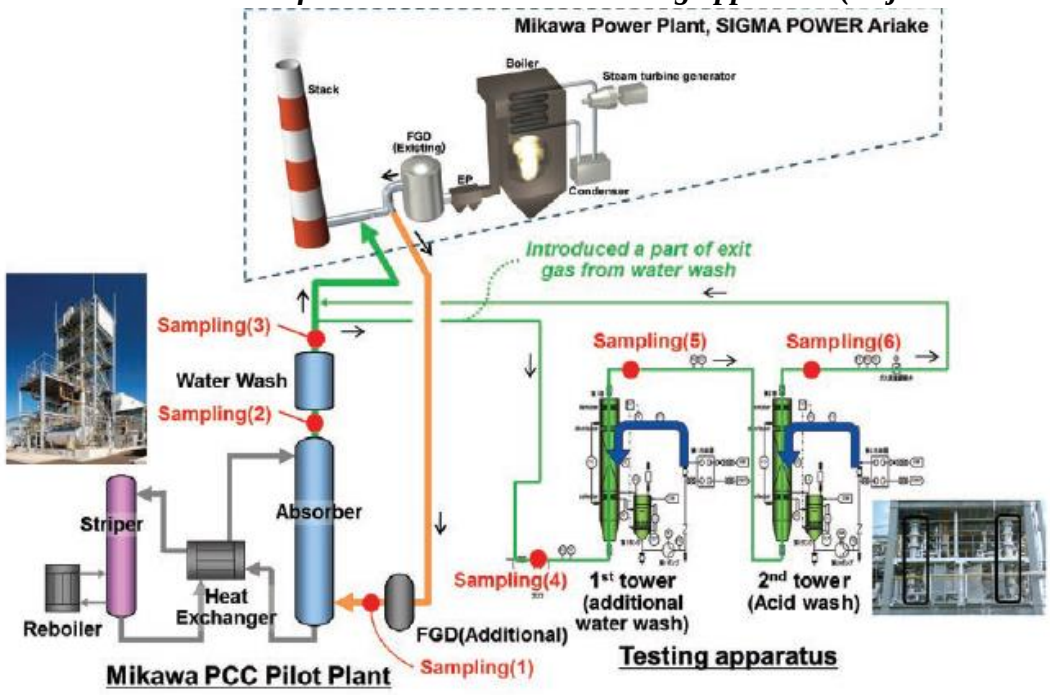

The PCC Pilot Plant was installed in Mikawa Power Plant, Japan (Figure 2.1.2). Actual flue gas for the pilot plant was introduced from the existing coal-fired power plant. The flue gas moved through the absorber and a water wash, and then was returned to the stack. In addition, approximately 5% of the exit gas from the water wash was directed to the testing apparatus consisting of the 1st tower (additional water wash) and the 2nd tower (acid wash) to study methods of further reduction of amine emissions.

There were six sampling points installed at the entrance and the exit of each unit of the pilot plant for measuring gas and particles.

***Figure 2.1.3: Illustration of On-line and Batch analytical methods for amine emissions (Fujita et al. 2017)***

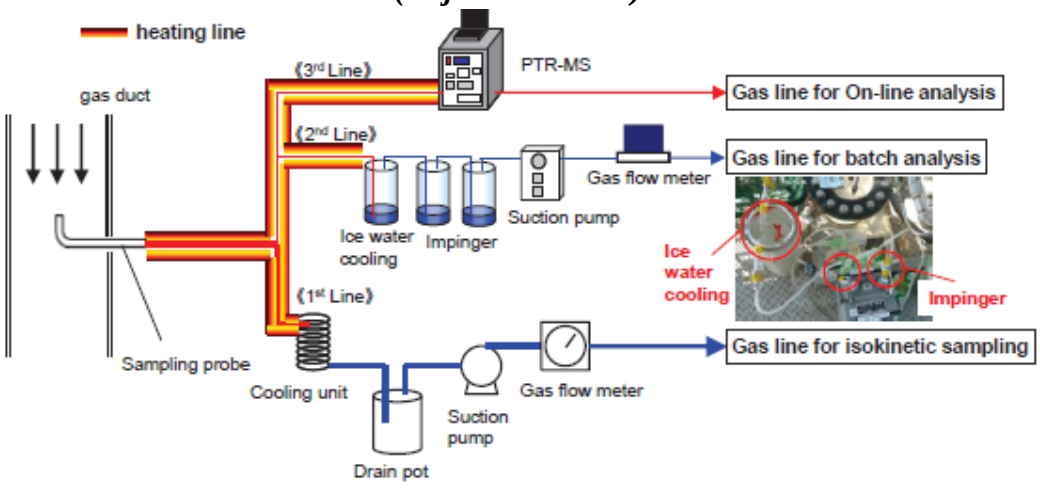


On-line and Batch analytical methods were utilised to measure the concentrations of amine in gas and aerosol phases. The sampling gas was divided into three gas lines (Figure 2.1.3.). The first line was used to adjust suction gas flow at the entrance of the sampling probe for isokinetic sampling. The second line (batch

analysis) was used to capture amines from the flue gas by ice water cooling and two impingers. Captured amines were measured by LC/MS/MS (TSQ Quantum Access Mass, Thermo Scientific) and GC/MS (GCMS-QP2010Ultra, Shimazu) and detected amine concentration to less than 10 ppb (v/v). The third line (on-line analysis) was used for supplying the sample gas into the Proton Transfer Reaction-Mass Spectrometry (PTR-MS, Ionicon Analytik GmbH), which detected amine concentration to less than 10 ppb (v/v).

Amine particles in 0.3-17.5 μm range contained in flue gas were detected by the particle spectrometer (Welas2070, PALAS GmbH). Particles of 10-470 nm range contained in flue gas at the entrance of absorber were detected by Scanning Mobility Particle Sizer Spectrometer (Model 3034 SMPSTM, TSI).

By comparing the results of Batch analysis and On-line analysis with respect to MEA, the differences between them were confirmed. Batch analysis gave the average concentration during two-hour sampling. It was observed that both analyses showed the same fluctuation tendency.

Plotting the highest-concentration amine measured at the exit from the absorber for both MEA and TS-1 solvents, showed that TS-1 has much better performance than MEA in terms of amine emissions.

It was found that the farther downstream the measured point is located, the lower amine concentration is reduced by water wash and acid wash. It was also found

that the higher the vapour pressure of amines is, the higher the washing rate is. It was suggested that particle-driven amine emissions are less likely to be reduced by the water wash and the acid wash, compared to vapour-driven amine emissions.

Investigation was carried out to observe how gas and liquid types fed into the absorber affect particle formation. It was found that feeding 30 wt.% MEA aqueous solution with air resulted in much higher particle number concentration than water with air. Furthermore, flue gas-30 wt.% MEA solution feed was compared to air-30 wt.% MEA solution feed. The flue gas case resulted in a dramatic increase in particle formation. The authors state that the increase in the number concentration of particles in the outlet is caused by the particles included in the flue gas.

How aerosol contained in the flue gas prior to entering the absorber impacts particle formation and growth was investigated. A remarkable increase in particle number concentration was observed at the outlet of the 1$^{st}$ tower followed by an increase in particle number concentration in the flue gas. The authors concluded that aerosol is a source of particle nuclei, and enhances particle growth inside the absorber.

The authors confirmed the hypothesis of particle growth by comparing peak diameters of particles in the inlet of the absorber and in its outlet. The fluctuation tendencies of the peak diameters were very close to each other.

## 2.2. Simulations

Imle et al. (2014) presented a method to predict supersaturation of the gas phase in absorption columns by rate-based modelling in Aspen Plus software. Predicting supersaturation is important because it drives particle formation. The influence of input parameters such as temperature of the inlet gas and solvent, and concentration of carbon dioxide in the inlet gas on supersaturation of the gas was studied by them. In their study only supersaturation was predicted, and particle formation was not modelled.

***Figure 2.2.1: Flowsheet used to predict supersaturation (Imle et al. 2014)***

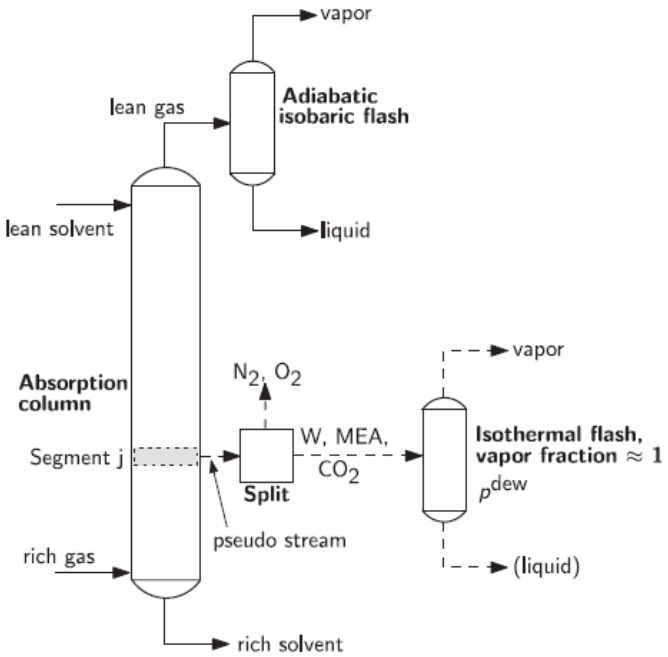


Flowsheet used in the study is shown in Figure 2.2.1. It includes the absorber, the isothermal flash to calculate the supersaturation profiles and the adiabatic flash used for determining the flowrate of the liquid formed by condensation.

To define supersaturation S of a gaseous mixture at given temperature and pressure, components of the mixture were classified as either condensable or non-condensable. According to Imle et al. (2014), a component was considered to be condensable "if it is found in the first droplet formed when the gas is compressed at constant temperature".

In this model, pseudo-streams were withdrawn from every segment of an absorption column. Pseudo-streams are absolute representatives of gas or liquid flow inside the column, but their flow does not disturb the mass or energy balance inside it.

The pseudo-stream was separated into condensable and non-condensable streams. The condensable stream was fed into an isothermal flash separator with the vapour fraction set to 0.9999. According to Imle et al. (2014), the corresponding pressure is a numerical approximation of the dew point pressure. To calculate S value of the pseudo-stream, Equation 2.2.1 was used.

$$S\,(T, p, y) = \frac{p \sum_{i=1}^{N_c} y_i}{p^{dew}(T, y^*)} \qquad (2.2.1)$$

Where S - supersaturation

T and p – temperature and pressure;

$N_c$ – number of condensable components;

y – mole fraction in a studied mixture;

y* - mole number in a "mixture of condensable components".

***Figure 2.2.2: Temperature and saturation profiles (Imle et al., 2014)***

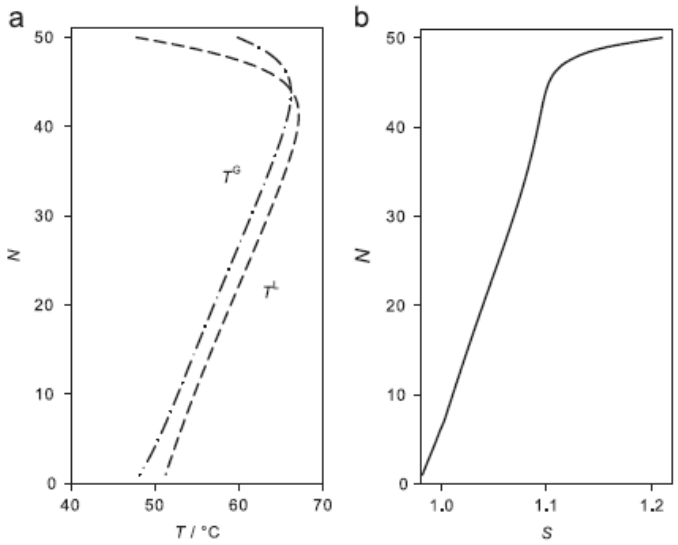


First, the base case was modelled and temperature and saturation profiles along the column were presented (Figure 2.2.2). The temperature of gas increased in the lower part of the column and decreased near its top as it was expected. In the saturation profile there was a gradual increase of supersaturation as the gas temperature became higher, and a drastic increase when the gas met cold solvent entering from the top. The gas became supersaturated (S>1) in the bottom of the column. The top supersaturation ratio was 1.21.

As expected, when the temperature of the rich gas increased, the supersaturation ratio decreased. When the temperature of the gas is increased, the dew point pressure of the mixture also increases. In addition, at higher temperatures solubility of $CO_2$ in aqueous MEA solution decreases and, thus, less heat is released during their reaction so that less water is evaporated. According to the Equation 2.2.1, supersaturation then decreases.

The temperature of the lean solvent has a strong influence on the top supersaturation ratio. The explanation is an increased temperature bulge at low lean solvent temperatures. At the same time, it was found that the lean solvent temperature has almost no effect on the supersaturation in the rest of the column.

It was found that variation of $CO_2$ content in the rich gas has a strong effect on supersaturation in the lower part of the column. In the upper part of the column, effect was smaller. The highest top supersaturation was reached by 0.04 g/g $CO_2$ concentration.

In the case when no $CO_2$ was present in the rich gas and in the lean solvent, no temperature bulge was observed as there was no exothermic reaction between MEA and $CO_2$. As a result, the top supersaturation reached just 1.01. Thus, no aerosol formation was expected in this case.

Khakharia et al. (2014a) developed a model in Aspen Plus V8.8 software to understand mechanisms of particulate matter formation and growth. They changed input parameters such as $CO_2$ content of the inlet flue gas, lean solvent temperature and lean solvent loading to understand their effect on particle based emissions.

***Figure 2.2.3. Schematic representation of modelling approach (Khakharia et al., 2014a)***

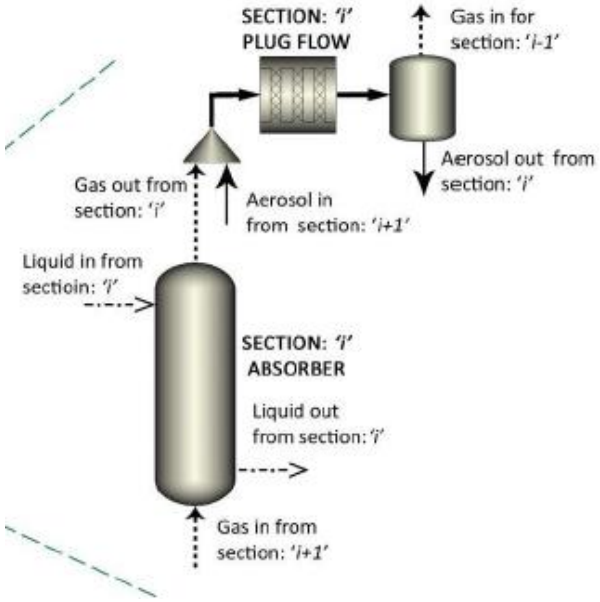


In their study absorber column was discretised into a number of sections. Figure 2.2.3 shows a schematic representation of the modelling approach for one section of the absorber. Each section was represented by an absorber column and a plug-flow reactor. Gas-solvent interaction was simulated in the absorber. Then, outlet gas from the absorber was mixed with particulate matter flow coming from the previous section on the bottom. The gas-particulate interaction was simulated in the plug-flow reactor after which the two phases were separated in a flash separator and sent to the following section on the top.

It was found that as the temperature of the flue gas increased along the column, so did its supersaturation ratio. The increase in the supersaturation occurred because of an increase in the partial pressure of volatile components such as MEA and water. At two-thirds of the column the gas reached the maximum temperature

and then started to cool down because of contacting cold solvent entering from the top. A drastic gas temperature decrease resulted in a significant increase in the supersaturation ratio. The supersaturation ratio profile followed the same trend as in the work by Imle et al. (2014). High supersaturation ratio results in high potential for particle formation and growth.

By varying $CO_2$ content in the inlet flue gas from 2 vol.% to 13 vol.%, it was found that reducing $CO_2$ content results in increase in supersaturation along the column. It was also found that higher $CO_2$ content results in higher top temperature of the gas. In turn, the top temperature is proportional to the amount of vapour MEA emissions. The highest amount of aerosol MEA emissions was found to occur at 10 vol.%, being a function of the supersaturation and the absolute top temperature. Aerosol emissions increase with temperature because of the increase in the concentration of volatile components available for transfer to aerosol phase. However, aerosol based emissions decrease at higher $CO_2$ concentrations because MEA activity in the solvent decreases.

Lean solvent temperature was varied from 30$^{o}$C to 50$^{o}$C, keeping the rest input parameters unchanged. At higher lean solvent temperatures, the top gas temperature increased as well, resulting in a lower temperature bulge. As a result, the top supersaturation ratio decreased. This finding is in accordance with Imle et al. (2014). This, in turn, results in that aerosol based MEA emissions decreased. However,

vapour MEA emissions increased at higher flue gas temperatures, but they can be removed by a conventional water wash.

By varying $CO_2$ loading of the lean solvent, it was found that the higher the loading, the lower the supersaturation ratio profile, especially at the top of the column. As a result, the corresponding aerosol MEA emissions also decreased at higher $CO_2$ loadings. Vapour emissions also decreased at higher $CO_2$ loadings.

Majeed et al. (2017a) developed a model in MATLAB to predict the development in particle size and particle internal variable profiles. The paper studied behaviour of a single particle moving along the absorber column.

The model of particle dynamics was represented by a system of partial differential equations, created in MATLAB.

The model, developed by Majeed et al. (2017a), included mass transfer equations for transferring components and the necessary diffusion reaction equations to describe the particle internal profiles. Also, it included heat transfer across the interface and inside the particle.

In the paper, there were several cases modelled with varying particle size and the initial composition of the particle, in terms of MEA concentration, to understand the behaviour of the particle inside the absorber. Some of the studied parameters are described below.

MEA and $CO_2$ concentration profile in the particle, and particle radius were checked for all cases. In all cases, MEA concentration increased while the particle was moving from the bottom of the column to the top. Whereas $CO_2$ concentration decreased in all cases. particle size for each case increased along the column after an initial decrease.

Increasing initial particle radius and maintaining initial MEA concentration low resulted in slightly higher MEA concentration at the exit from the column. This increase occurred because the particle surface area increased resulting from the radius increase. As a result, more MEA was transferred to it.

$CO_2$ concentration profile was also almost similar in all cases reaching at the outlet values close to zero.

Particle size profiles all followed the same trend. They all experienced a decrease in the very bottom of the column due to water evaporation, and then a continuous increase until the top of the column due to MEA and water transport into the particle. At the very top, particle s in all cases slightly decreased in size due to the temperature decrease and MEA and water transport out of the particle.

Majeed et al. (2017b) work is an extension of Majeed et al. (2017a) work. In this study, the effect of amine depletion in the gas phase was taken into account.

The system of differential balance equations was created simulating component mass and energy inside the particle and gas phases. These equations were

used with a reaction model, an equilibrium model and models between for heat and mass transfer between the gas and the solvent phases and between the gas and the aerosol phases.

In the paper, there were several cases modelled with varying particle size and the initial composition of the particles, in terms of MEA concentration, to understand how various particle number concentrations (from 1 to $10^7$ per $cm^3$) affect the gas phase composition. Some of the obtained results are described below.

It was found that for large particle number concentrations partial pressures of MEA in the gas phase increase from the bottom of the column to the upper zone. However, in the upper zone, the MEA partial pressure decrease until the outlet. Partial pressure of water in the gas phase follows the same trend as MEA. Both profiles are dependent on the temperature inside the absorber. As the temperature increases, condensable components evaporate from the solvent to the gas phase. When it decreases at the upper zone, MEA and water evaporation rate decreases.

### 2.3. Literature review conclusion

Based on the works reviewed in this chapter, several conclusions can be made to understand what has been done in the area of particle formation and growth, and what the current study can bring in to better understand mechanisms of particle formation and growth.

In the experimental studies reviewed, the focus was on particle size and number concentration at the outlet of the absorber. However, nothing has been reported on particles behaviour inside absorber columns yet. Thus, the results on particles behaviour inside absorbers, obtained in simulations, cannot be validated by experiments.

The model for defining supersaturation ratio of a gaseous mixture developed by Imle et al. (2014) was utilised in the present work. In comparison to the present study, Imle et al. (2014) only predicted and tested supersaturation ratio, whereas particulate formation was not modelled.

Khakharia et al. (2014a) used a plug-flow reactor to simulate gas-particle interaction. Plug-flow reactors simulate only reactions between the components. However, they do not provide information on mass and heat transfer between the gas and the particles.

Majeed et al. (2017a) studied component profiles only for a single particle and for gas phase. It was assumed that gas phase composition is not affected by the particle phase.

Component profiles for gas at high particle number concentrations were studied in Majeed et al. (2017b). However, component profiles for particles at high number concentrations were not considered. They implemented the same approach as in this work by estimating mass and heat transfer rates between the gas and the

particle phases. However, they only studied gas-particle interaction, whereas simultaneous gas-solvent interaction was not considered. In addition, Majeed et al. (2017b) did not develop any flowsheet simulation model within a commercial software such as Aspen Plus to make it available for commercial applications.

To date, no studies have been developed to estimate the nucleation rate inside absorber columns.

The present work aimed to further develop the simulation studies that were reviewed in this chapter by introducing a new conceptual model to estimate heat and mass transfer rates between gas and particulate phases using Aspen Plus simulation software. Another objective was to validate the model by comparing it with results of an experimental mini-plant developed by TNO group in Netherlands.

# Chapter 3 - Conducted Work and Research

## 3.1. Model development

### 3.1.1. Model

Aspen Plus V9.0 software was used in this study. The particulate phase flows from the bottom to the top of the column co-currently with the gas phase. Existence of particle flow means that the third phase must be introduced into the absorber column as the interaction between all three phases occurs simultaneously. However, in Aspen Plus, this cannot be done in a straightforward manner.

In order to simplify and simulate the real condition, the model developed by Khakharia et al. (2014a) was further improved. The process was split into two steps. In the first step, the gas phase contacts counter-currently with the solvent in an absorber column modelled using a rate-based approach. Then, the treated gas meets particle phase in another absorber column modelled using a rate-based approach. In this column, the particle phase and the gas phase contact counter-currently, but the modelling, as explained later, is set up in a way that a co-current contact is taken into account.

***Figure 3.1.1.1. Schematic diagram of the absorber and the aerosol column for one stage***

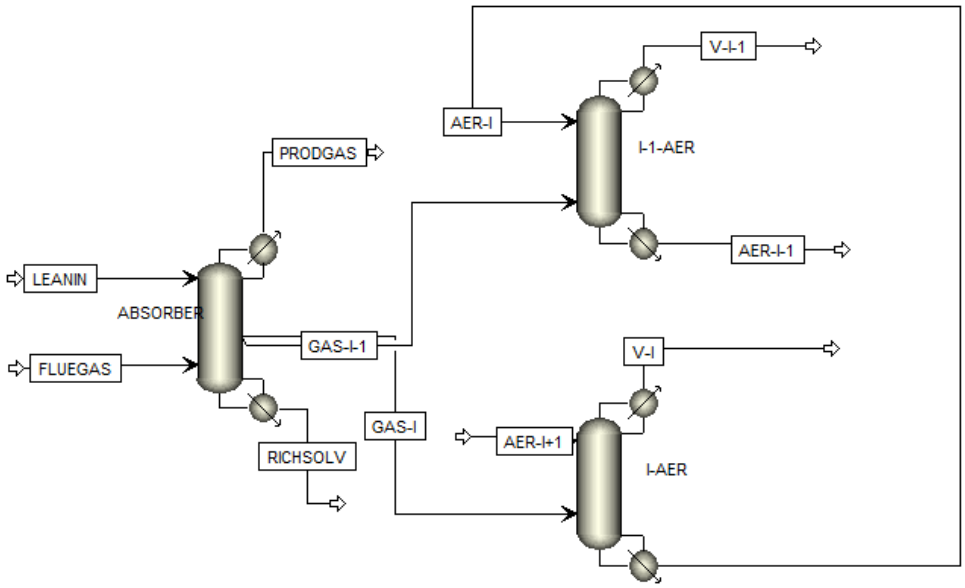


The schematic diagram of the model is illustrated in Figure 3.1.1.1. For modelling the first step of the process, a single absorber was developed consisting of 25 stages to represent 5 sections of the experimental mini-plant. 25 pseudo-streams were taken from the absorber, representing the gas outlet from each stage. Pseudo streams have same temperature, pressure, flowrate and composition as the gas inside the column. However, they do not disturb mass and energy balance inside the column.

For modelling the second step of the process, there were other 25 absorbers (aerosol columns) set in the model. They represented 25 sections of the experimental absorber of the mini-plant. Each pseudo-stream entered a respective aerosol column, consisting of two stages, where gas-particle interaction was simulated. Particle phase acted as a solvent in the aerosol columns. The aerosol columns were connected to

each other by the flow of particle phase from the column on the bottom to the column on the top.

### 3.1.2. Thermodynamics

To model interaction between gas and particles, and between gas and solvent, a rate-based modelling was considered. Electrolyte-NRTL (ELECNRTL) thermodynamic package in Aspen Plus was used to estimate the physical properties and phase equilibrium. This is similar to what is provided in Aspen Plus "Rate-Based Model of the $CO_2$ Capture Process by MEA" example (Aspen Technology, Inc, 2014). The existing pure component and binary interaction parameter data in the Aspen Properties databank was not changed. Henry's law was used to obtain the solubility of supercritical components such as $CO_2$, $N_2$, $O_2$, CO, $H_2$.

### 3.1.3. Correlations

For the absorber column, where gas and solvent interaction was simulated, Aspen built-in correlations were used for mass transfer coefficient and for interfacial area. In both cases the Bravo et al. (1985) correlation method was used. For heat transfer coefficient in both absorber and aerosol columns the Chilton and Colburn analogy was used.

## 3.2. Conceptual model

The next step was to develop a set of equations for creating a new conceptual model to estimate heat and mass transfer rates between gas and particulate phases as

no experimental mass transfer correlations exist for gas streams flowing co-currently with solid or liquid particles in a packed column (Khakharia et al., 2014a). The new model is based on the two-film theory, that was suggested by Whitman in 1923 (Seader and Henley, 1998) for separation processes that involve contacting two fluid phases. According to the two-film theory, "each film presents a resistance to mass transfer, but concentrations in the two fluids at the interface are in equilibrium" (Seader and Henley, 1998, p.150).

The two-film theory allows to predict the mass transfer between two fluid phases across an interface, assuming that equilibrium exists at the interface. It enables to model the interaction between the gas and the particle phases accurately.

It is assumed that the particles have an ideal spherical shape. The model considers only gas-solvent and gas-particle interaction, assuming that the solvent and the particle phases do not interact with each other. In the current model, it is also assumed that the gas and the particles move with same velocity. Thus, they are stationary relative to each other.

In order to estimate mass transfer between the gas and the particles, the interfacial area and the mass transfer coefficient must be calculated. To do so, the area available for the gas-particle contact must be calculated. The volume of the particles flowing through the absorber section was divided by the number of the particles in it to find volume of a single particle and its radius in this section. Having

found the particle radius, the surface area of all particles and, thus, the gas-particle mass transfer can be computed for a particular section of the absorber.

The mathematical basis of the new conceptual model is described in Sections 3.2.1 and 3.2.2. The new model is applied to each of 25 aerosol columns through the use of internal Fortran subroutine available in Aspen Plus.

First, number of particles in each of 25 sections of the absorber was calculated. Equation 3.2.1 was used for estimation of particle number in the absorber section (i) (unitless):

$$PMN = PMNC \times VOL_i \qquad \text{Equation 3.2.1}$$

Where PMN is the total particle number in each section of the column. PMNC is the particle number concentration. PMNC inside the flue gas entering the column was obtained from the measurements performed at the mini-plant at TNO to be $4.8\times10^7$ particles/cm$^3$. As no experimental values are reported for the particle number concentration development along the column, PMNC was assumed to be constant along the absorber. This assumption is fairly acceptable as the particle nucleation occurs mainly on the surface of the existing particles, and not much significant changes in the particle number concentrations will occur. $VOL_i$ represents the free volume of the given column section through which the gas flows.

### 3.2.1. Interfacial area

For computing the interfacial area in each section of the absorber, Flowsheeting Option such as Calculator Block was created and set for each aerosol column. Figure 3.2.1.1 shows how Calculator Block looks. In the calculator block, a set of equations for each section was written, enabling Aspen Plus to compute the interfacial area in each section of the absorber. All variables, that were used or calculated, were defined in advance.

***Figure 3.2.1.1: Calculator block screenshot***

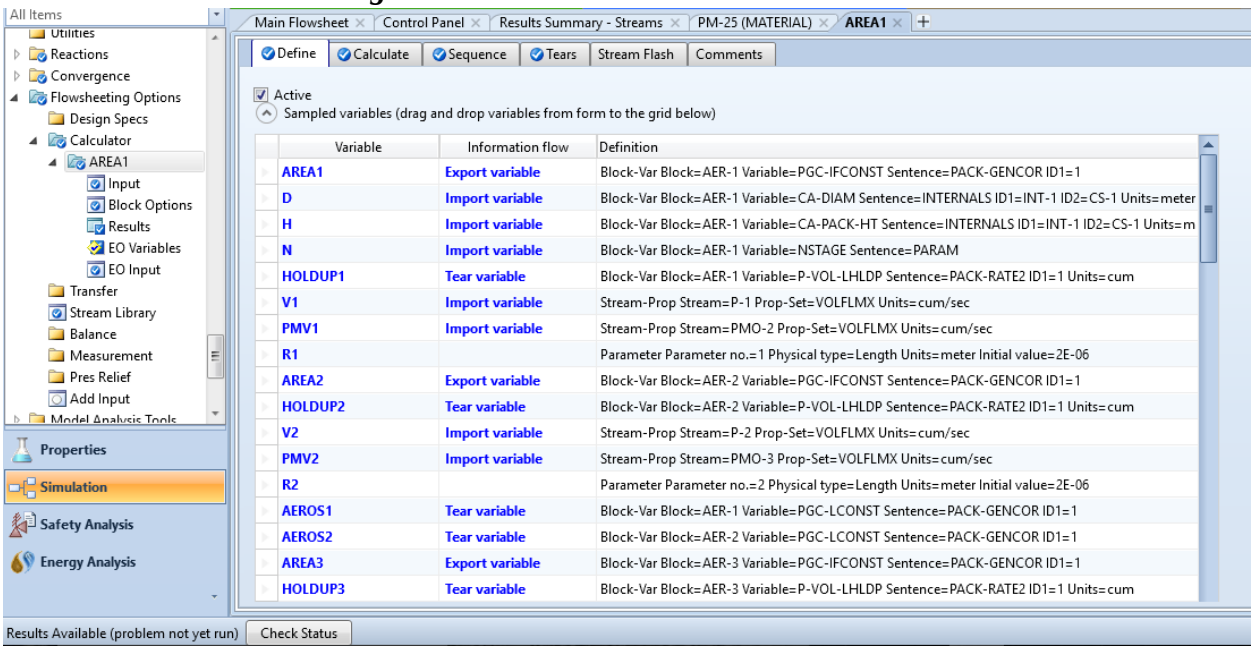


All defined variables are shown in Table 3.2.1.1 below, where subscript (i) is for the section number.

***Table 3.2.1.1: Defined variables for calculator block "Area"***

| Variable | Information flow | Description | Unit |
|---|---|---|---|
| $Area_i$ | Export | Ratio of the specific interfacial area to the packing specific area | - |
| D | Import | Column diameter for the section | m |
| H | Import | Packed height for the section | m |
| N | Import | Number of theoretical stages, incl. condenser and reboiler | - |
| $Holdup_i$ | Tear | Liquid holdup for liquid phase kinetic reactions on a volume basis | $m^3$ |
| $V_i$ | Import | Volumetric flowrate of the gas inlet to the column | $m^3/s$ |
| $PMV_i$ | Import | Volumetric flowrate of the liquid inlet to the column | $m^3/s$ |
| $R_i$ | | Aerosol particle radius | m |
| $Aeros_i$ | Tear | Liquid Sherwood number | - |

Next step was to develop a set of equations to calculate the export variable:

1. Particles number in each absorber section (no unit)

$$PMN = 3.28136 \times 10^{11}$$

2. Equation for finding liquid holdup in each section, i.e. volume taken by particle phase (unit: $m^3$)

$$HOLDUP_i = \frac{PMN \times 4 \times \pi \times R_i^3 \div 3}{N}$$

3. Equation for finding volume of the section available for gas (unit: $m^3$)

$$VOL_i = (\pi \times (\frac{D}{2})^2 \times H) - HOLDUP_i$$

4. Equation for finding time for the gas to pass a given section of the absorber (unit: s)

$$T_i = \frac{VOL_i}{V_i}$$

5. Equation for finding the radius of a particle in the given section of the absorber (unit: m)

$$R_i = \left(\frac{(PMV_i \div PMN) \times T_i \times 3}{4 \times \pi}\right)^{1/3}$$

6. Packing material specific surface area, provided by its manufacturer (unit: $m^2/m^3$)

$$a = 492$$

7. Equation for finding the ratio of the specific interfacial area to the packing specific area for the generalised interfacial area correlation equation (no unit)

$$AREA_i = \frac{PMN \times 4 \times \pi \times R_i^2}{\pi \times (D \div 2)^2 \times H \times a}$$

### 3.2.2. Mass transfer coefficient

To find the mass transfer coefficient, Sherwood number for solvent and gas passing over a particle in each section of the absorber must be calculated. For this purpose, the calculator block was further developed.

Sherwood number for liquid

Defined variables are same as shown in Table 3.2.1.1.

Set of equations for calculating the liquid Sherwood number is as follows:

1. Sherwood number is defined as

$$Sh = \frac{k \times L}{D}$$

Where k – convective mass transfer film coefficient (m/s),

L – characteristic length (m)

D – mass diffusivity ($m^2/s$)

2. Convective mass transfer film coefficient is defined as follows

$$k = \frac{D}{\sigma}$$

Where D - mass diffusivity ($m^2/s$)

σ – film thickness (m)

3. Rearranging gives

$$Sh = \frac{D \times L}{D \times \sigma} = \frac{L}{\sigma}$$

4. Column diameter, $D_C$ can be used for the characteristic length. Film thickness was assumed to be equal to the radius of the particle, R. Thus,

$$Aeros_i = \frac{D_C}{R_i}$$

5. Equation for finding volume of the section available for gas (unit: $m^3$)

$$VOL_i = (\pi \times (\frac{D}{2})^2 \times H) - HOLDUP_i$$

6. Equation for finding time for the gas to pass a given section of the absorber (unit: s)

$$T_i = \frac{VOL_i}{V_i}$$

7. Equation for finding the radius of a particle in the given section of the absorber (unit: m)

$$R_i = (\frac{(PMV_i \div PMN) \times T_i \times 3}{4 \times \pi})^{1/3}$$

Sherwood number for vapour

Frossling equation for finding Sherwood number is as follows (Rousseau, 1987, p.114):

$$Sh_V = 2 + 0.6 \times Re^{1/2} \times Sc^{1/3}$$

Where Re – Reynolds number,

Sc – Schmidt number.

As gas and particulate matter are assumed to be stationary relative to each other, Reynolds number becomes zero, and Sherwood number equals two.

### 3.2.3. Assumptions

1. Solvent and particulate phases do not interact with each other.
2. No coagulation and decay of particles is considered.
3. No nucleation
4. Particles and gas flow co-currently with same velocity

### 3.3. Input parameters

Absorber column parameters, and solvent, flue gas and particulate inlet parameters were set to imitate a real experimental carbon capture mini-plant developed and tested by TNO group in Netherlands.

In the experimental mini-plant the flue gas containing particles is generated in several steps. In the beginning, $SO_2$ gas reacts with air in a reactor. Then, the product of this reaction consisting of $SO_3$ gas and air is transferred to a quenching column where $H_2SO_4$ is formed as a result of reaction between $SO_3$ and cold water. At the outlet of the quencher there is a mixture of PM and air. This stream is then mixed with the flue gas stream and directed into the absorber column.

Inlet stream conditions are specified in Tables 3.3.1, 3.3.2, 3.3.3 and 3.3.4.

***Table 3.3.1: Inlet streams parameters***

| Parameter | Flue gas | Solvent | Particle |
|---|---|---|---|
| Temperature (°C) | 44 | 40 | 44 |
| Pressure (bar) | 1.12485 | 1.58325 | 1.12485 |
| Flowrate (kmol/h) | 0.173004 | 0.612741 | $2.49199\times10^{-5}$ |

***Table 3.3.2: Flue gas inlet flowrates***

| Component | Value | Unit |
|---|---|---|
| $N_2$ | 2765 | l/h |
| $O_2$ | 735 | l/h |
| $CO_2$ | 500 | l/h |
| $H_2O$ | 40 | g/h |

***Table 3.3.3: Lean solvent inlet flowrates***

| Component | Value | Unit |
|---|---|---|
| MEA | 4.2 | kg/h |
| $H_2O$ | 9.8 | kg/h |
| $CO_2$ | 0.63 | kg/h |

The lean solvent is a 30 wt.% MEA aqueous solution with $CO_2$ loading of 1.46 mol $CO_2$/kg $H_2O$.

***Table 3.3.4: Particle inlet composition***

| Component | Mass fraction |
|---|---|
| $H_2O$ | 0.1917 |
| $H_3O^+$ | 0.2508 |
| $OH^-$ | 0.2278 |
| $H_2SO_4$ | 0.1161 |
| $HSO_4^-$ | 0.1063 |
| $SO_4^{2-}$ | 0.1073 |

The PM entering the column was assumed to contain water and sulphuric acid only. The sulphuric acid content was set in such away, that there were 45 mg $H_2SO_4/Nm^3_{gas}$. The exact composition of the PM inlet stream was computed by Aspen Plus. The procedure to estimate the PM stream inlet volumetric flowrate by using information from the experimental mini-plant is presented below.

During the experiment, the particles entering the experimental absorber were classified according to their diameters from 0.006 to 5.3 μm. Then, the particle number concentration for each group of diameters was measured (0 to $2\times10^7$ $cm^{-3}$). Next, the number flowrate of each group of the particles was estimated as the product of particle number concentration (PMNC) by the flue gas flowrate. The number

flowrate of each group was then multiplied by the volume of a single particle and summed up to obtain the volumetric flowrate of the PM stream. The volumetric flowrate of the particulate matter was found to be $1.59012\times10^{-10}$ $m^3/s$.

The experimental absorber contained 5 sections each with 5 units of Sulzer laboratory BX packing. Each unit was 170 mm height. Above the liquid inlet to the column there was an additional section with 1 unit of 170 mm height packing, which served as insulation between the column and the environment.

To simulate the experimental absorber, absorber and aerosol columns specification, shown in Tables 3.3.5 and 3.3.6, was used. It was assumed that the experimental mini-plant absorber consisted of 25 stages as stage specification is required in Aspen Plus. The additional section above the liquid inlet cannot be incorporated in the absorber directly in Aspen Plus. Therefore, the gas outlet of the top aerosol column was directed to a flash unit operating at the same temperature and pressure as the gas stream to separate its vapour from liquid. Then, the obtained vapour stream was sent to another flash unit operating at the temperature and pressure that were measured experimentally in the gas exiting from the additional packing section. The vapour outlet of this flash unit represented the gas leaving this packing section, whereas the liquid outlet represented the vapour that condensed due to cooling and returned back to the column.

***Table 3.3.5: Absorber column specification***

| Parameter | Value |
|---|---|
| Total packing height (m) | 4.25 |
| Diameter (m) | 0.045 |
| Stages (-) | 25 |
| Packing type (-) | BX Sulzer Standard |
| Packing material (-) | Standard |

***Table 3.3.6: Aerosol columns specification***

| Parameter | Value |
|---|---|
| Sectional packing height (m) | 0.17 |
| Diameter (m) | 0.045 |
| Stages in section (-) | 2 |
| Packing type (-) | BX Sulzer Standard |
| Packing material (-) | Standard |

## 3.4. Chemistry and thermodynamic reactions

The chemistry and reaction sets, used in the current study, are same as provided in "Rate-Based Model of the $CO_2$ Capture Process by MEA" example (Aspen Plus, 2014). They are shown in tables 3.4.1 and 3.4.2 respectively. The only modification was addition of sulphuric acid dissociation into the chemistry set for particle simulation.

Equilibrium constants were computed by minimisation of Gibbs energies by Aspen. The parameters for kinetic reactions were provided by the Aspen Plus example (Appendix A).

***Table 3.4.1: Chemistry set***

| Rxn No. | Reaction type | Stoichiometry |
|---|---|---|
| 1 | Equilibrium | $2H_2O \leftrightarrow H_3O^+ + OH^-$ |
| 2 | Equilibrium | $CO_2 + 2H_2O \leftrightarrow HCO^{3-} + H_3O^+$ |
| 3 | Equilibrium | $HCO^{3-} + H_2O \leftrightarrow CO_3^{2-} + H_3O^+$ |
| 4 | Equilibrium | $MEAH^+ + H_2O \leftrightarrow MEA + H_3O^+$ |
| 5 | Equilibrium | $MEACOO^- + H_2O \leftrightarrow MEA + HCO^{3-}$ |
| 6 | Equilibrium | $H_2SO_4 + H_2O \leftrightarrow H_3O^+ + HSO_4^-$ |
| 7 | Equilibrium | $HSO_4^- + H_2O \leftrightarrow H_3O^+ + SO_4^{2-}$ |

***Table 3.4.2: Reactions set***

| Rxn No. | Reaction type | Stoichiometry |
|---|---|---|
| 1 | Equilibrium | $MEAH^+ + H_2O \leftrightarrow MEA + H_3O^+$ |
| 2 | Equilibrium | $2H_2O \leftrightarrow H_3O^+ + OH^-$ |
| 3 | Equilibrium | $HCO_3^- + H_2O \leftrightarrow CO_3^{2-} + H_3O^+$ |
| 4 | Kinetic | $CO_2 + OH^- \rightarrow HCO_3^-$ |
| 5 | Kinetic | $HCO_3^- \rightarrow CO_2 + OH^-$ |
| 6 | Kinetic | $MEA + CO_2 + H_2O \rightarrow MEACOO^- + H_3O^+$ |
| 7 | Kinetic | $MEACOO^- + H_3O^+ \rightarrow MEA + CO_2 + H_2O$ |

In this study, total MEA refers to MEA, $MEAH^+$ and $MEACOO^-$, collectively.

### 3.5. Supersaturation

The saturation degree of a pure component in a mixture is reported in the literature to be (Seinfield and Spyros, 2015):

$$S = \frac{p_i(y,T)}{p_{eq}(y,T)} \qquad \text{Eq. (3.5.1)}$$

where p is partial pressure of a condensable component i, $p_{eq}$ is the saturation vapour pressure (dew pressure) of that component in equilibrium at temperature T.

According to Seinfield and Spyros (2015), the precondition for PM formation through homogeneous nucleation is satisfied when Equation 3.5.1 predicts supersaturation for a given mixture (S>1). There is no need for individual saturation values to exceed 1 for nucleation to take place in systems with several condensing components (Seinfield and Spyros, 2015). Moreover, for systems that contain more than one condensable component, Equation 3.5.2 is applied (Gretscher and Schaber, 1999):

$$S = \frac{P_C\,(T,y_1,y_2,\ldots y_n)}{P_{CS}(T,y_1,y_2,\ldots y_n)} \qquad \text{Eq. (3.5.2)}$$

where $P_C$ is the total partial pressure of all condensing vapour components at the actual temperature $T$ and mole fraction, $y_i$ of the supersaturated gas, and $P_{CS}$ is the total partial pressure of all the condensing components corresponding to the phase equilibrium. Nevertheless, the extension of Equation 3.5.1 to Equation 3.5.2

does not have strong scientific support and may not be sufficient to observe the supersaturation in a mixture containing several condensing components.

In this work, the method developed by Imle et al. (2014) was utilised in order to estimate the saturation ratio of the gas inside the absorber column. A gas pseudo stream, withdrawn from each stage of the absorber column, was directed to a flash unit, that operated at constant temperature and a vapour fraction of 0.9999. As a result, the mixture at the outlet of the flash unit had the pressure that represented the $P_{CS}$ in Equation 3.5.2.

# Chapter 4 – Results and Discussion

## 4.1. Absorber temperature profiles

***Figure 4.1.1: Temperature profile inside absorber obtained from experiment and simulation***

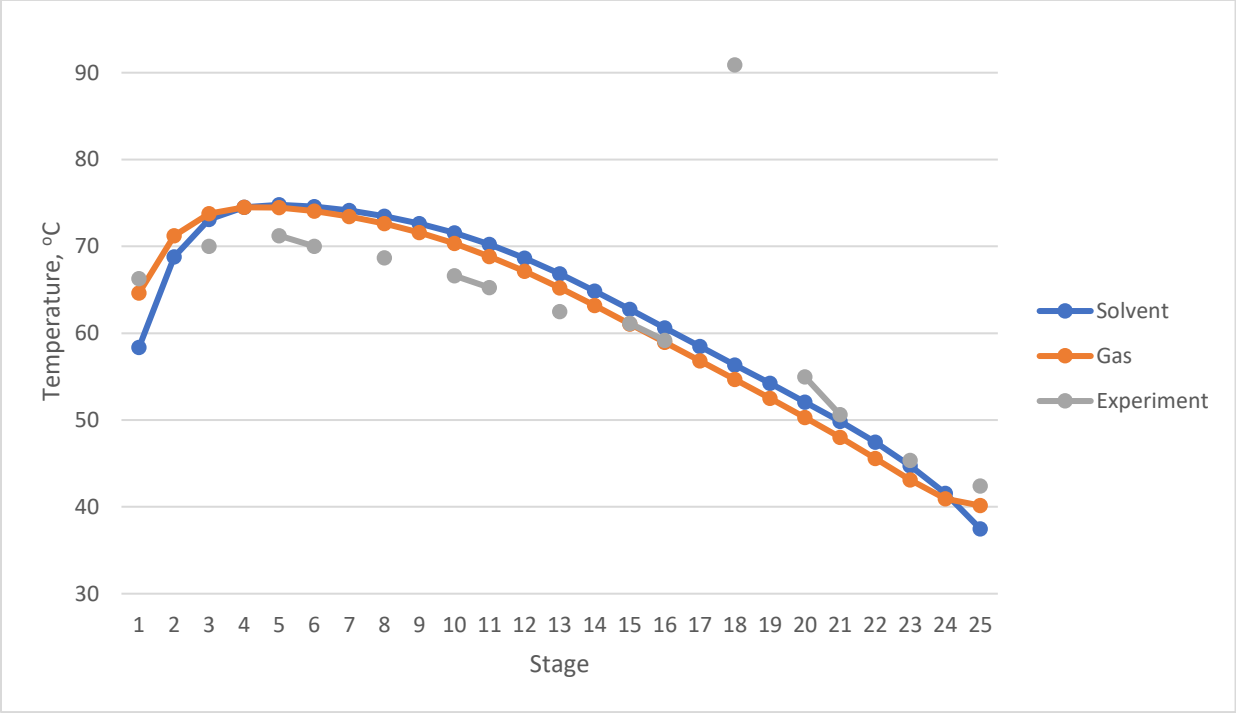


Figure 4.1.1 above illustrates the temperature profiles of the gas and the solvent inside the absorber column that were obtained during the model simulation (legends “Gas” and “Solvent” respectively). The “Experiment” legend shows the temperature profile measured inside the absorber during the experiment.

During the experiment, temperature of 91°C was measured in the lower half of the absorber, probably, due to some accidental inaccuracy of failure of a thermometer. Generally, as it can be seen from the graph, the simulation and experimental profiles are reasonably close to each other and follow the same trend.

The obtained profiles are typical for $CO_2$ absorption process. Similar temperature profiles were obtained in experiments (Khakharia et al., 2013) and simulations (Imle et al., 2014, Khakharia et al., 2014a). Temperature of the gas increases while it moves from the bottom of the column up to stage 4 due to exothermic nature of reaction between $CO_2$ and MEA. In the region above stage 4, the temperature goes down because of a leading effect of heat transfer from the gas to the cold solvent entering from the top. The temperature difference between the maximum flue gas temperature and its temperature at the top of the absorber is known as the temperature bulge. (Khakharia et al., 2013)

## 4.2. MEA, $H_2O$ and $CO_2$ mole flows in gas and particle phases

***Figure 4.2.1. Total MEA mole flow in particle and gas phases***

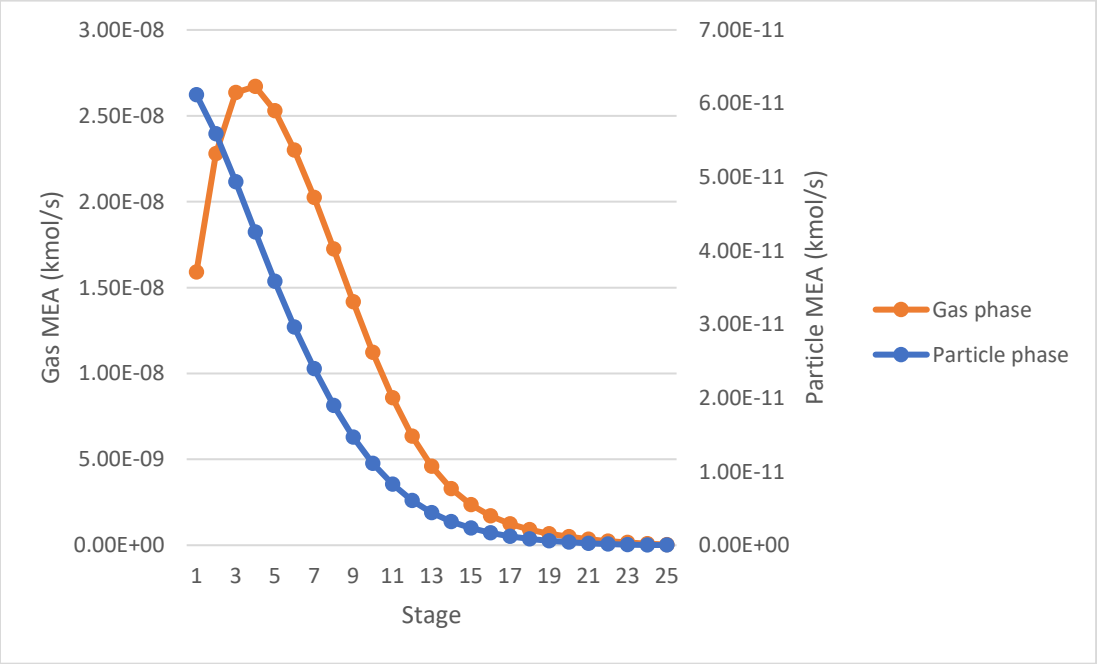

Figure 4.2.1 shows that MEA mole flowrate in the particle phase gradually increases along the column. The same result was obtained by Majeed et al. (2017a). It increases because the gas and the particle phases interact with each other while moving from the bottom of the column to the top. As the temperature increases, MEA from the solvent evaporates, and then it is transferred from the gas to the particles. At the outlet of the absorber MEA flowrate in the particle phase was estimated to be $6.12\times10^{-11}$ kmol/s or 0.28 mg/Nm$^3$. Hereinafter, the normal condition for the gas was considered to be 293.15 K and 101325 Pa.

MEA mole flow profile in the gas phase is also illustrated in Figure 4.2.1. It follows the same trend as the partial pressure profile of MEA in the gas phase studied by Majeed et al. (2017b). MEA mole flow in gas gradually increases from the bottom of the column up to stage 4. Then it decreases significantly until the top of the packing, reaching $1.59\times10^{-8}$ kmol/s or 751 mg/Nm$^3$. This profile can be related to the temperature profile inside the absorber. As the temperature increases, MEA evaporates and transfers to the gas phase. When the temperature decreases at the top of the column, amount of MEA evaporated decreases.

***Figure 4.2.2: MEA mass transfer between the solvent and the gas along the absorber-Positive values represent mass transfer from vapor to the solvent phase***

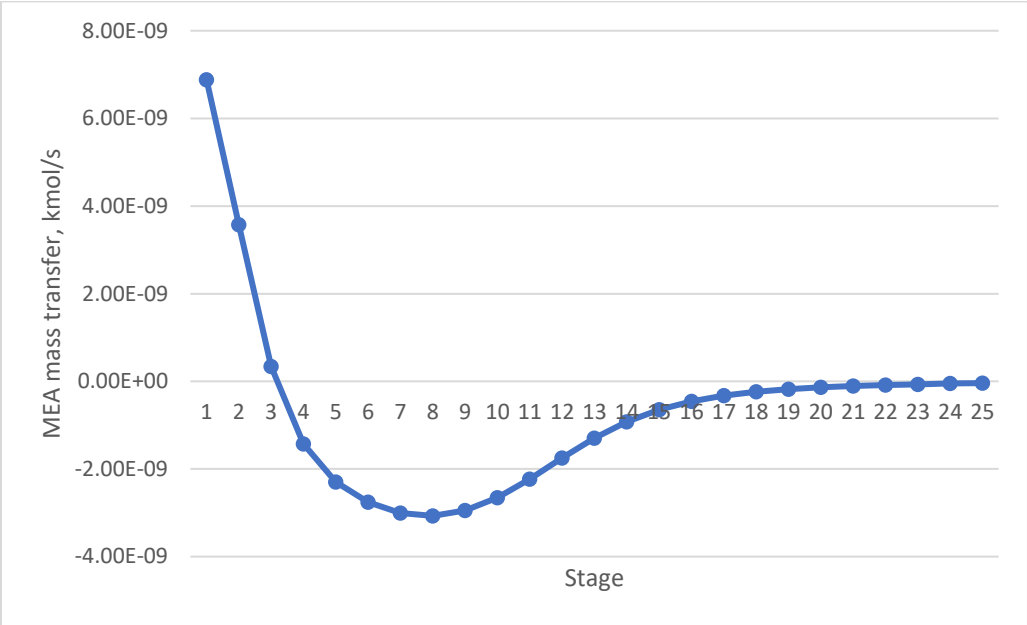


MEA mass transfer rate between the solvent and the gas phase along the column is presented in Figure 4.2.2. MEA transfers from the solvent to the gas from stage 25 to stage 3. The mass transfer rate increases from stage 25 to stage 10, but then it decreases from stage 8 to stage 4. As of stage 3, the mass transfer rate direction changes from the gas to the solvent with an increasing trend toward stage 1.

The MEA profile in the gas phase can also be related to $CO_2$ loading of the amine solution. At the bottom stages, the MEA solution is more loaded with $CO_2$, as it captured it on its way from the top to the bottom of the column. As a result, at the bottom of the column MEA has lower partial pressure in the gas phase.

As was mentioned, there was an additional packing section installed above the liquid inlet to the column that served as an insulation resulting in the exit gas temperature decrease from 68°C to 53°C. When the temperature of the gas decreases, a certain fraction condenses and flows back to the column in the form of liquid, which has MEA in it. The rest of the gas exits the column. It was found that the gas cooled to 53°C has just 1.32 mg MEA/Nm$^3$.

***Figure 4.2.3: Total $H_2O$ mole flow in the particle and the gas phases***

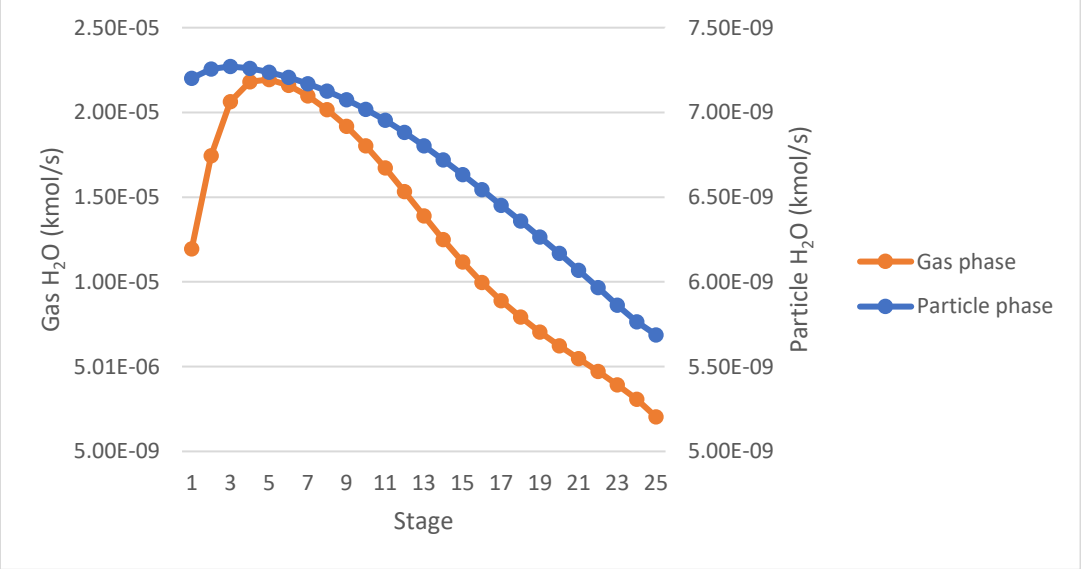


Figure 4.2.3 shows water mole flowrate in the gas and the particle phases. In the gas phase the water mole flowrate strongly depends on the temperature profile. As the temperature increases, water evaporates from the solvent and transfers to the gas phase. At the top of the column, as the temperature decreases, the water condenses back to the solvent. The same profile was obtained for partial pressure of $H_2O$ development along the absorber by Majeed et al. (2017b). The flowrate in the

particle phase steadily increases along the column and reaches its maximum at stage 3, then it slightly decreases until stage 1. The mole flowrate of water in the particle phase depends on amount of water that is transferred to it from the gas phase. As at the top of the absorber mole flowrate of water in the gas phase decreases, less water is transferred to the particle phase.

***Figure 4.2.4. Water mass transfer between the solvent and the gas along the absorber-Positive values represent mass transfer from vapor to the PM phase***

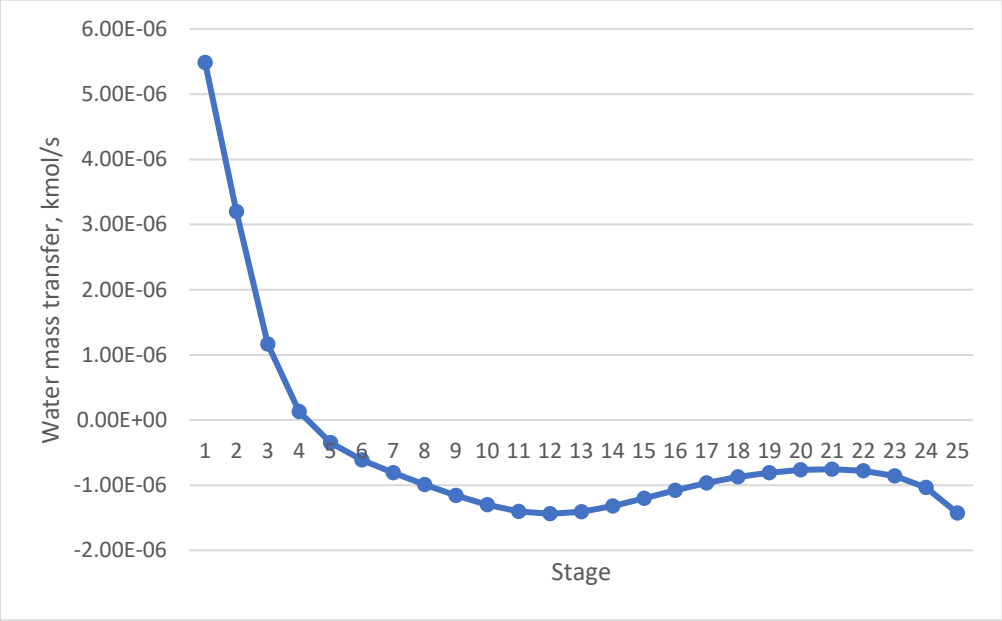


The water mass transfer rate from the solvent to the gas (Figure 4.2.4) fluctuates from stage 25 to stage 5. However, as of stage 4, the transfer direction reverses from the gas to the solvent with an increasing trend.

***Figure 4.2.5: Total $CO_2$ mole flow in the particle and the gas phases***

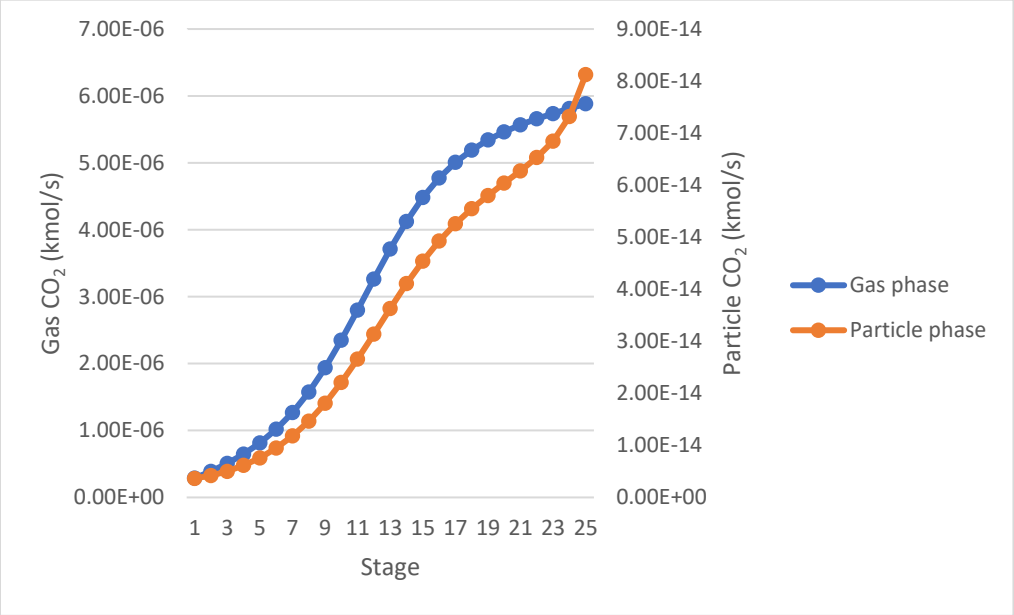


$CO_2$ mole flowrate in the gas and the particle phase, shown in Figure 4.2.5, decreases gradually while moving to the top of column. The mole flowrate of $CO_2$ in the particle phase depends on amount of $CO_2$ that is transferred to it from the gas phase. As along the column mole flowrate of $CO_2$ in the gas phase decreases, less $CO_2$ is transferred to the particle phase. Both profiles follow the same trend as presented in the works by Majeed et al. (2017a) and Majeed et al. (2017b).

Another reason for $CO_2$ mole flow in the particle phase decrease along the column can be its reaction with MEA to form $MEACOO^-$. However, it can be seen on Figure 4.2.6 that flow of MEA is not affected by this reaction due to large difference in flowrates. Consequently, $CO_2$ mole flow might not be affected too.

***Figure 4.2.6: MEA and $MEACOO^-$ mole flow along the column in particle phase***

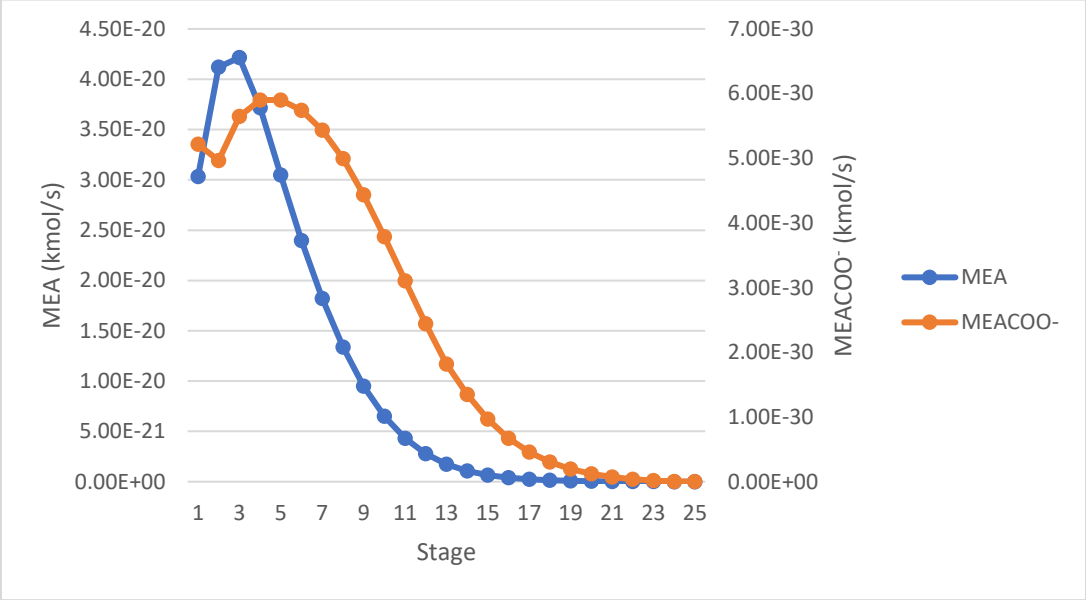


## 4.3. $CO_2$ removal efficiency

***Table. 4.3.1: Mini-plant and simulation results for $CO_2$ removal efficiency***

| | Removal efficiency (%) |
|---|---|
| Mini-plant | 85.2 |
| Simulation | 95.1 |

As it can be seen from Table 4.3.1, the two values of $CO_2$ removal efficiency are not very close to each other. The relative difference between the values is approximately 11.6%.

## 4.4. Gas particles saturation

***Figure 4.4.1: Gas particles saturation inside absorber***

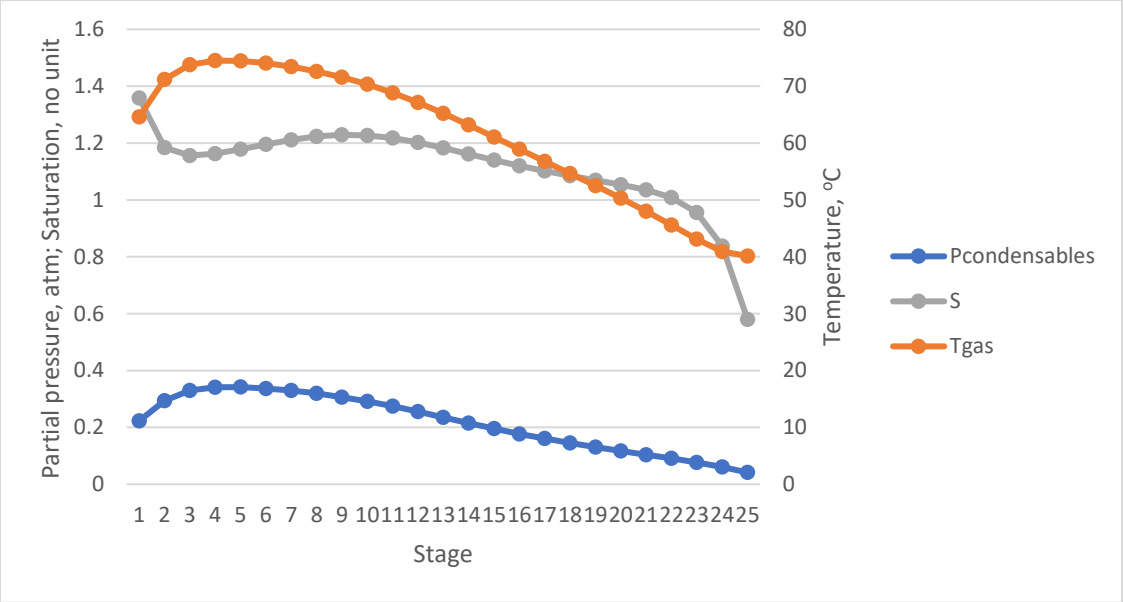


The development of the gas particles saturation along the absorber and its relation to the absorber temperature profile and partial pressure of condensable components (water and MEA) is shown in Figure 4.4.1. The saturation profile trend is similar to the results obtained by Imle et al. (2014) and Khakharia et al. (2014a).

The S trend informs that the gas saturation increases almost continuously. It starts from 0.58 at stage 25 and becomes supersaturated at stage 22 with S = 1.01. Then the gas supersaturation continues to rise until stage 9 (S=1.23). This rise is due to the temperature increase inside the absorber and the subsequent increase in partial pressures of water and MEA. According to Khakharia et al. (2014a), the gas temperature increase along the column “leads to increase in the partial pressure of volatile components such as water and MEA”.

Along stages 9 to 3, gas supersaturation decreases reaching the local minimum value of 1.16. The decrease mainly occurs because the temperature increase rate slowed down, and the partial pressures of volatile components stopped increasing and started to decrease.

At stages 2 and 1 the gas phase meets cold solvent. As a result, the temperature of the gas drops from 73.8$^{o}$C at stage 3 to 71.2$^{o}$C at stage 2 and to 64.6$^{o}$C at stage 1. Temperature bulge at the top of the absorber results in the gas becoming colder than the solvent. Therefore, the gas saturation ratio in this area increases significantly (Khakharia et al., 2014a). As a result, the gas saturation jumps to S = 1.36 at stage 1.

Saturation and consequent supersaturation can contribute to the particle growth in size. As it was already mentioned, when a particle becomes supersaturated, “nuclei are formed by molecules of condensing components and/or on the impurities in the flue gas” (Khakharia et al., 2014a). This is referred to homogeneous and heterogeneous nucleation respectively. It means that when heterogeneous nucleation takes place, condensing components, such as MEA and water, attach to the existing aerosol particles and, thus, the size of particles increases. Whereas when homogeneous nucleation occurs, then new aerosol particles appear by condensed components.

## 4.5. Particle total volumetric flowrate

*Figure 4.5.1: Particle volumetric flowrate profile*

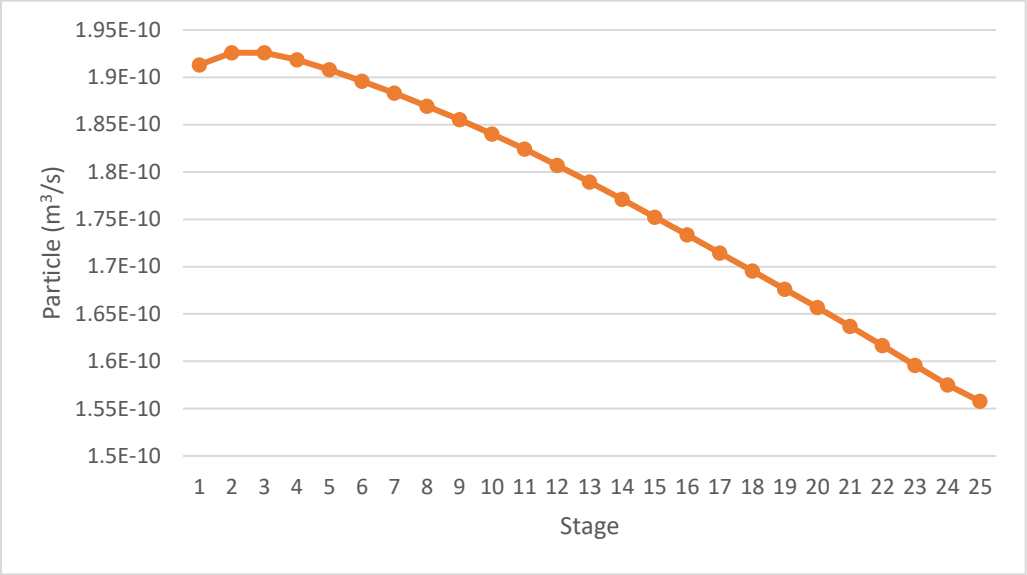


Particle total volumetric flowrate continuously increases from the bottom of the column up to stages 2 and 3. It then slightly decreases at stage 1 (Fig. 4.6.1). An increase in mole flow of condensable components, such as MEA and water, in the particle phase results in total particle flowrate increase. As water mole flow in the particle phase is two orders of magnitude higher than that of MEA, it has more effect on total particle volumetric flowrate.

This finding is in accordance with the work by Mertens et al. (2014), that states that particles grow inside the absorber due to the uptake of MEA and water by particles.

## 4.6. Dependence of outlet gas and aerosol MEA on particle inlet flowrate

***Figure 4.6.1: Outlet gas and aerosol MEA (mg/Nm$^3$) vs inlet particle volumetric flowrate (m$^3$/s)***

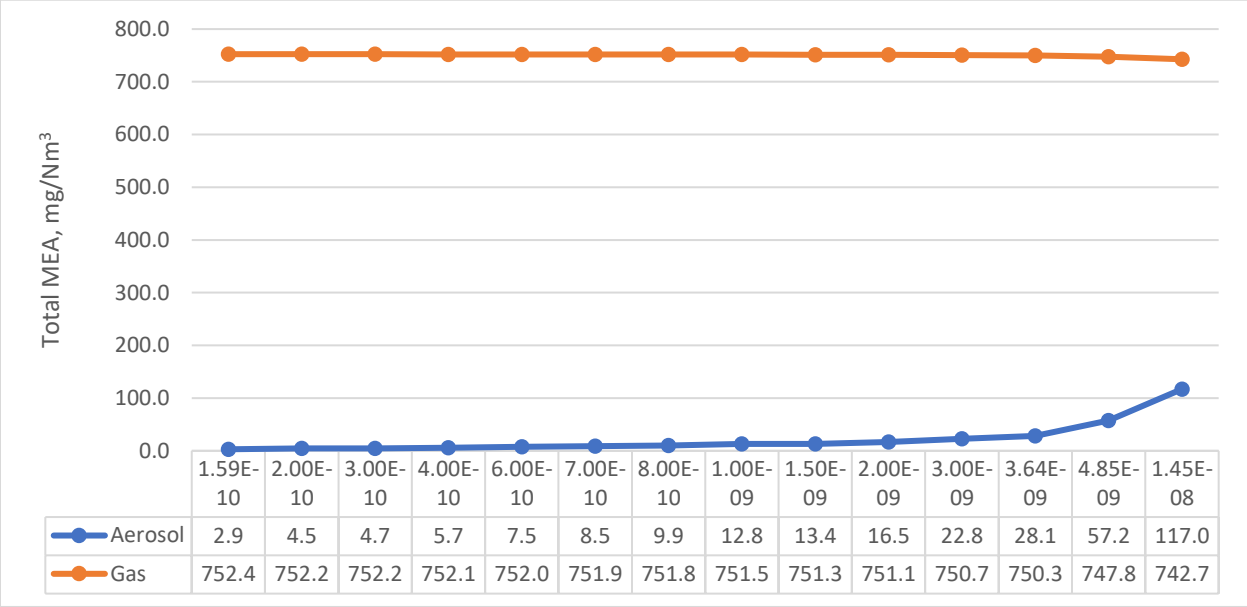


| | 1.59E-10 | 2.00E-10 | 3.00E-10 | 4.00E-10 | 6.00E-10 | 7.00E-10 | 8.00E-10 | 1.00E-09 | 1.50E-09 | 2.00E-09 | 3.00E-09 | 3.64E-09 | 4.85E-09 | 1.45E-08 |
|---|---|---|---|---|---|---|---|---|---|---|---|---|---|---|
| Aerosol | 2.9 | 4.5 | 4.7 | 5.7 | 7.5 | 8.5 | 9.9 | 12.8 | 13.4 | 16.5 | 22.8 | 28.1 | 57.2 | 117.0 |
| Gas | 752.4 | 752.2 | 752.2 | 752.1 | 752.0 | 751.9 | 751.8 | 751.5 | 751.3 | 751.1 | 750.7 | 750.3 | 747.8 | 742.7 |

According to Khakharia et al. (2014a), particle MEA concentration in the outlet gas can reach several grams per Nm$^3$. However, in the current study particle MEA concentration is in the order of several mg per Nm$^3$. To understand the result obtained and its cause, the plot shown on Figure 4.6.1 was created.

It can be seen from Figure 4.6.1 that there is a dependence of outlet particle MEA concentration on inlet particle volumetric flowrate. Based on the information shown in Figure 4.6.1, it can be noticed that the relation might be hyperbolic. Evidently, the trend will continue at higher inlet particle flowrates.

This phenomenon can occur because higher flowrate of the PM phase increases its mass transfer rate. To confirm this hypothesis, MEA mass transfer rate from gas to particles estimated at the top stage by Aspen Plus was compared at

different PM inlet flowrates. In the baseline case, when the PM inlet volumetric flowrate was $1.59012\times10^{-10}$ $m^3/s$, the MEA mass transfer from the gas phase to the particle phase was $5.3\times10^{-12}$ kmol/s. In comparison, when the PM inlet volumetric flowrate was increased to $2.5\times10^{-9}$ $m^3/s$, the MEA mass transfer from gas to particles became $3.58\times10^{-11}$ kmol/s. At the PM inlet flowrate of $3.927\times10^{-7}$ $m^3/s$, MEA mass transfer was $1.71\times10^{-9}$ kmol/s.

## 4.7. Dependence of gas and particle MEA profiles on $H_2SO_4$ initial concentration

***Figure 4.7.1: Gas and particle MEA profiles***

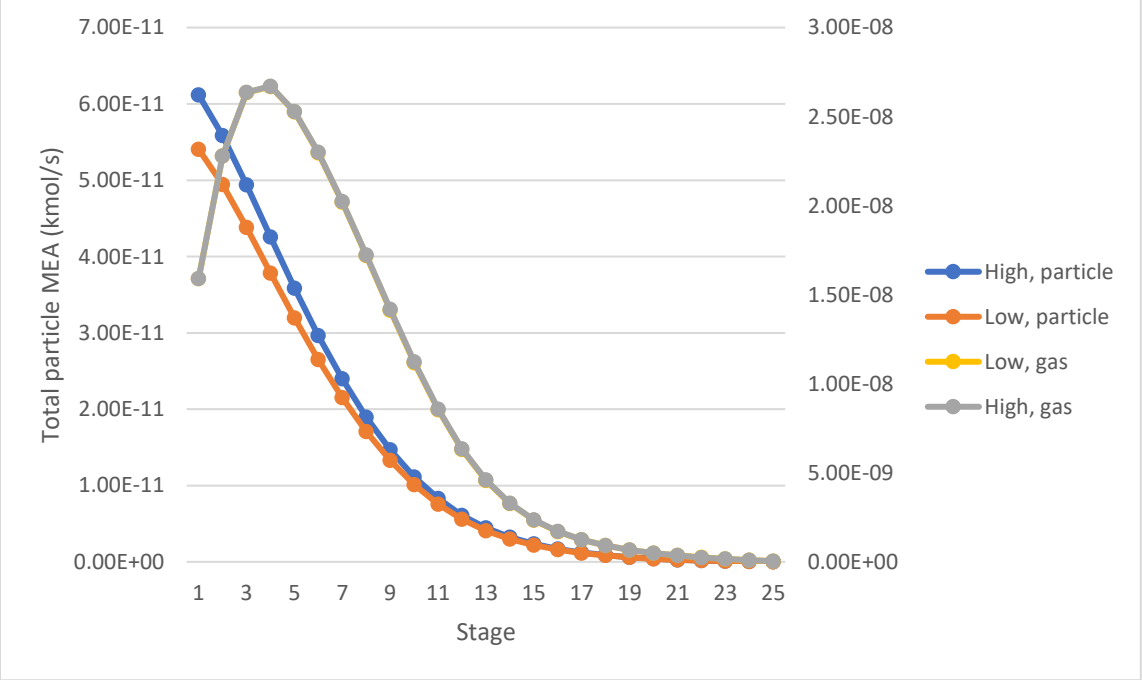


Figure 4.7.1 illustrates gas and particle MEA profiles along the absorber at two levels of $H_2SO_4$ concentration in the inlet flue gas: high (45 $mg/Nm^3$) and low (12 $mg/Nm^3$).

It can be seen that the high initial $H_2SO_4$ concentration results in slightly higher profile of total particle MEA along the absorber than the low initial $H_2SO_4$ concentration. Particle MEA emission at the outlet of the absorber at high $H_2SO_4$ concentration was observed to be $6.12\times10^{-11}$ kmol/s. At low $H_2SO_4$ concentration it was found to be $5.41\times10^{-11}$ kmol/s. At high inlet $H_2SO_4$ concentration the MEA mass transfer rate from the gas to the particle phase in the top aerosol column was approximately $3.24\times10^{-12}$ kmol/s. At low inlet $H_2SO_4$ concentration, the MEA mass transfer rate was approximately $2.82\times10^{-12}$ kmol/s. It can be noted that the increase in MEA emission is not as significant as increase in $H_2SO_4$ concentration. In comparison, the gas phase MEA emission was found to be independent of the $H_2SO_4$ concentration in the inlet flue gas as in both cases the profiles copy each other.

## 4.8. Particle size profile along the column

***Figure 4.8.1. Particle size profile along the column***

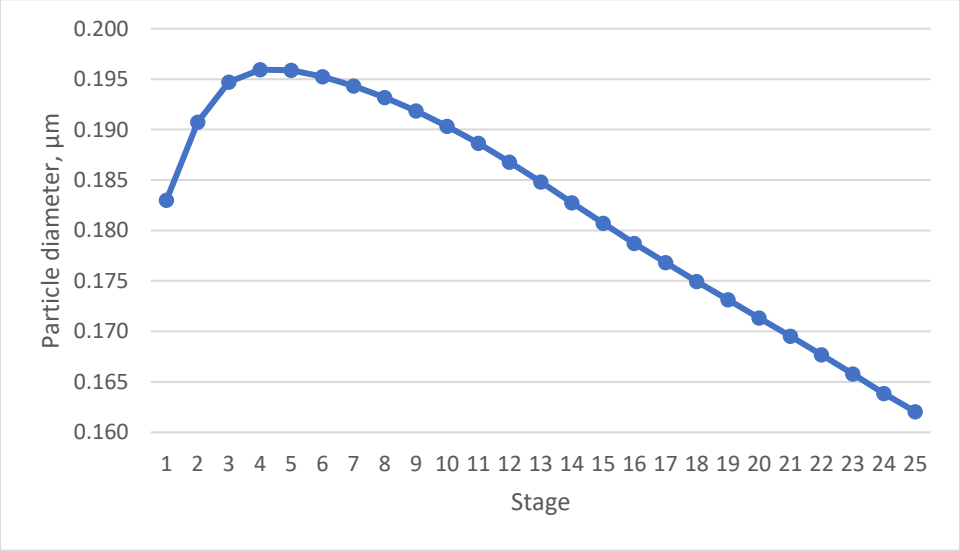

Figure 4.8.1. shows that the particle size gradually increases as it enters the absorber column up to stage 4. At stage 25 the particle size was 0.162 μm. At stage 4 it reached 0.196 μm. Then the size of particles slightly decreases until the top of the column reaching the size of 0.183 μm at the top stage. If mass size distribution was studied experimentally, this particles size would be representative of the mode particle diameter.

Comparing Figure 4.8.1 with Figures 4.2.1 and 4.2.3 shows relation between particle diameter and the mole flows of MEA and water in the PM phase. As the mole flow of condensable components, such as MEA and water, in the particle phase increases along the column, the particle size also grows. As the water mole flow in the particle phase is two orders of magnitude higher than that of MEA, it has a higher effect on the particle diameter. In addition, the total particle volumetric flowrate increases along the column (Figure 4.5.1) as a result of particle size increase.

The particle size profile is similar to what was found in literature. In particular, Majeed et al. (2017a) found that particles decrease in size slightly at the bottom and the top of the column, and significantly increase along the main body of the column.

## 4.9. Total MEA concentration in combined gas and particle phase

***Table 4.9.1: Mini-plant and simulation results for total MEA concentration in combined gas and particle phase***

| | Steady state value (mg/Nm$^3$) | Range (mg/Nm$^3$) |
|---|---|---|
| Mini-plant | 595 | 590 - 600 |
| Simulation | 754 | - |

As it can be seen from Table 4.9.1, the total MEA concentration value in the combined gas and particle phase at the outlet of the absorber from the simulation and the experiment are the same order of magnitude. The relative error is approximately 27%. However, when there were no particle nuclei in the flue gas, the MEA emission was 150 mg/Nm$^3$. Therefore, particle contribution to the MEA emission from the mini-plant at steady-state operation was 445 mg/Nm$^3$. These values sharply differ from what was found in this simulation (1.32 mg/Nm$^3$ and 0.28 mg/Nm$^3$ respectively). The gas phase MEA concentration found experimentally can be higher than that found in simulation because a certain fraction of the MEA, condensed in the packing section above the liquid inlet, can be picked up by the gas to the exit from the column. The difference in the particle phase MEA concentration can occur because of nucleation phenomenon, which is discussed in the following section. Moreover, the differences can arise because experimental measurements of the MEA emission is a difficult task and could be subject to measurement uncertainties (Khakharia et al., 2014b).

### 4.10. Nucleation rate

In theory, minimisation of the Gibbs energy of a supersaturated gas at constant temperature and pressure results in saturation of the gas, and subsequent formation of new particulate matter from the excess mass leaving the gas phase (Seinfield and Spyros, 2016). The formed PM and the remaining gas are then in equilibrium. The obtained mass of the particulate matter can be estimated as the sum of the masses produced through two mechanisms: molecular mass trasnfer to the preexisting particles and the mass transfer due to the cluster formation (nucleation). In the present study, a rate-based model was implemented to estimate mass transfer between the supersaturated gas and the particles in aerosol columns. This mass transfer is understood to be molecular mass transfer because existing theoretical and empirical mass transfer correlations in literature typically estimate the molecular mass transfer rather than nucleation mass transfer. Therefore, there is a possibility to improve results of the current study by taking into account MEA loss due to nucleation. In this regard, the Gibbs energy of the vapour stream leaving the top aerosol column was minimised by directing it to a flash unit in Aspen Plus, operated at the same temperature (337.78 K) and pressure (1 atm) of the vapour stream. The flash unit produced the total liquid mass of $1.92414\times10^{-6}$ kg/s. The estimated total mass transfer rate from the gas phase at the top of the absorber column to the particle phase was found to be $-7.3\times10^{-10}$ kg/s, indicating net mass transfer direction from

the particle to the gas phase. Thus, the mass transfer due to the nucleation was estimated to be approximately ($1.92414\times10^{-6}$ kg/s - ($-7.3\times10^{-10}$ kg/s) $1.92487\times10^{-6}$ kg/s, representing an estimate of the total particle formation due to nucleation. If the diameter of the particles leaving the column is 0.183 μm, then the estimated nucleation rate would approximately be $2\times10^{15}$ particles.$cm^{-3}.s^{-1}$, respectively.

In general, depending on the method used to estimate the nucleation rate, their values can range over several orders of magnitude (Diemand et al., 2013, Sosso et al., 2016). Experimental value for nucleation rate of water is found to be three orders of magnitude less than the value obtained by classical nucleation theory (CNT) (Sosso et al., 2016). Seven orders of magnitude difference was reported between the value found in the study of homogeneous nucleation of water in an argon media using molecular dynamics (MD) simulation, performed by Yasuoka and Matsumoto, and the theoretical value (Yasuoka et al., 1998a). MD simulations were also used in another study by Yasuoka and Matsumoto to estimate nucleation rate of water at 350K (Yasuoka et al., 1998b). The nucleation rate was identified to be $4.21\times10^{29}$ $cm^{-3}s^{-1}$, whereas the value calculated using CNT was $3.7\times10^{28}$ $cm^{-3}s^{-1}$. Nucleation rate for $CO_2$ at 269 K was reported by Horsch et al. (2008) to be $4.1\times10^{27}$ $cm^{-3}s^{-1}$, and the value predicted by CNT was $2.5\times10^{27}$ $cm^{-3}s^{-1}$. To summarise, CNT model values for nucleation rate differ from experimental values by up to 26 orders of

magnitude, whereas MD simulation results in up to 14 orders of magnitude difference from experimental values (Sosso et al., 2016).

The nucleation values, reported in this study, should not be considered as an exact value of the nucleation rate for such a system. Currently, there are no experimental and modelling nucleation data for such a multicomponent mixture in the absorption column. Hence, the nucleation rate estimated in this work can serve as a starting point to improve the simulation results using commercial software that exclude nucleation rate in their calculations.

In this work, it was attempted to correct the estimated MEA loss through the PM phase. The flowrate of the total MEA in the flash liquid outlet stream ($8.15893\times10^{-7}$ kg/s) was considered as the MEA formed due to the nucleation and molecular mass transfer. Using the rate-based method, the MEA mass transfer rate from the gas phase to the particle phase due to the molecular diffusion (mass transfer) was estimated to be $3.25\times10^{-10}$ kg/s. Hence, the mass transfer due to the nucleation was estimated to be $8.15568\times10^{-7}$ kg/s. Given the nucleation mass transfer for MEA and the gas flowrate inside the aerosol column, the total MEA emission through the PM due to the nucleation is estimated to be 696.98 mg/Nm$^3$. Finally, the particulate phase total MEA concentration (molecular and nucleation mass transfer rates) is estimated to be (0.28 mg/Nm$^3_{gas}$ + 696.98 mg/Nm$^3_{gas}$) 697.3 mg/Nm$^3_{gas}$.

# Chapter 5 - Conclusion and Future Work

The new conceptual model to estimate heat and mass transfer rates between gas and particulate phases using Aspen Plus simulation software presented in this work was successfully validated with the results of the experimental carbon capture mini-plant. The model simulation was used in order to estimate MEA loss through the particle phase and factors that influence it.

Particle formation and growth is a complex phenomenon that depends on multiple factors. High temperature inside the absorber results in evaporation of MEA from the solvent to the gas phase, and, subsequently, in its transfer to the particle phase. Temperature bulge in the upper zone of the absorber results in the supersaturation jump just before the exit from the column and a subsequent condensation of MEA on particles' surface. Transfer of condensable components to the particle phase results in the increase in the particle size and volumetric flowrate along the column. When the inlet flowrate of particle phase increases, particle phase MEA emissions increase because more MEA is transferred to particles. Increasing $H_2SO_4$ concentration in the inlet gas also results in particle phase MEA emission increase.

Definitely, aerosol phenomenon needs continuous research to better understand mechanisms of particle formation and growth. Similarly to other studies,

Equation 3.5.2 was employed in this work to predict the saturation ratio of a condensable mixture. Equation 3.5.2 is the extension of Equation 3.5.1 but for a multicomponent mixture. However, this extension does not have strong scientific support. One concern regarding Equation 3.5.2 is that particle nucleation can occur at S values below 1. In addition, Equation 3.5.2 estimates nucleation of the whole condensing mixture, resulting in a multicomponent PM phase. A detailed study is required in future to evaluate reliability of Equation 3.5.2.

Different particle size distribution can be used along the column if such kind of information is available from experiments. Another issue of this study was its inability to predict particle decay on their way through the column. Namely, particle coagulation and particle attachment to the inside surfaces of the column are expected. Particle coagulation takes place when particle number concentrations increase such that particles start to coagulate and grow in size but not in mass. Particle attachment occurs when particles attach to inner surfaces of the column, such as wall and mechanical parts. Finally, the current model does not estimate particle nucleation rates. If such information is found from experiments or modelling, then it can be integrated in this model to obtain more accurate results.

# List of References

Abu Zahra, M. R. M. 2009. *Carbon dioxide capture from flue gas. Development and evaluation of existing and novel process concepts.* Ph. D. thesis. Delft University of Technology.

Alie, C., Backham, L., Croiset, E. and Douglas, P. L. 2005. Simulation of $CO_2$ capture using MEA scrubbing: a flowsheet decomposition method. *Energy Conversion and Management*. **46**, pp. 475-487.

Aspen Technology, Inc. 2014. Rate-Based Model of the $CO_2$ Capture Process by

MEA using Aspen Plus. Available from: http://home.aspentech.com/products/engineering/aspen-plus

Brachert, L., Mertens, J., Khakharia, P. and Schaber, K., 2014. The challenge of measuring sulfuric acid aerosols: number concentration and size evaluation using a condensation particle counter (CPC) and an electrical low pressure impactor (ELPI+). *Journal of Aerosol Science.* **67**, pp. 21–27.

Bravo, J.L., Rocha, J.A. and Fair, J.R., 1985. Mass transfer in gauze packings. *Hydrocarbon processing*, **64** (1), pp.91-95.

Da Silva, E.F., Kolderup, H., Goetheer, E., Hjarbo, K.W., Huizinga, A., Khakharia, P., Tuinman, I., Mejdell, T., Zahlsen, K., Vernstad, K., Hyldbakk, A., Holten, T., Kvamsdal, H.M., van Os and P., Einbu, A. 2013. Emission studies from a CO2 capture pilot plant. *Energy Procedia.* **37**, pp. 778–783.

Diemand, J., et al., *Large scale molecular dynamics simulations of homogeneous nucleation.* The Journal of Chemical Physics, 2013. **139**(7): p. 074309.

Fujita, K, Muraoka, D., Kaseda, T., Saito, S., Kitamura, H., Kato, Y., Udatsu, M., Handa, Y. and Suzuki, K. 2017. Impact of the aerosol particle included in actual flue gas on amine mist formation/growth in the Post-Combustion Capture Pilot Plant. *Energy Procedia*. 114, pp. 930-938.

Fulk, S. M., Beaudry, M. R., Rochelle, G. T. 2017. Amine Aerosol Characterization by Phase Doppler Interferometry. *Energy Procedia*. 114, pp. 939-951.

Gretscher, H. and Schaber, K. 1999. Aerosol formation by heterogeneous nucleation in wet scrubbing processes. *Chemical Engineering and Processing*. **38**, pp. 541–548.

Horsch, M., et al., *Homogeneous nucleation in supersaturated vapors of methane, ethane, and carbon dioxide predicted by brute force molecular dynamics.* The Journal of Chemical Physics, 2008. **128**(16): p. 164510.

IEA Clean Coal Center. 2007. *Post-combustion carbon capture from coal fired plants – solvent scrubbing*. Available from: http://www.iea-coal.org.uk/documents/81793/6448/Carbon-capture

Imle, M., von Harbou, E., Brachert, L., Schaber, K. and Hasse, H. 2014. Predicting supersaturation by rate-based simulations of reactive absorption. *Chemical Engineering Science*. **118**, pp. 41-49.

Khakharia, P., Brachert, L., Mertens, J., Huizinga, A., Schallert, B., Schaber, K., Vlugt, T. G. H. and Goetheer, E. 2013. Investigation of aerosol based emission of MEA due to sulphuric acidaerosol and soot in a Post Combustion $CO_2$ Capture process. *International Journal of Greenhouse Gas Control.*

Khakharia, P., Mertens, J., Vlugt, T. J. H. and Goetheer, E. 2014a. Predicting Aerosol Based Emissions in a Post Combustion $CO_2$ Capture Process Using an Aspen Plus Model. *Energy Procedia.*

Khakharia, P., M Kvamsdal, H., da Silva, E.F., Vlugt, T.J.H. and Goetheer, E. 2014b. Field study of a Brownian Demister Unit to reduce aerosol based emission from a Post Combustion $CO_2$ Capture plant. *International Journal of Greenhouse Gas Control.* **28**, pp. 57-64.

Khakharia, P., Brachert, L., Mertens, J., Anderlohr, C., Huizinga, A., Fernandez, E. S., Schallert, B., Schaber, K., Vlugt, T. G. H. and Goetheer, E. 2015. Understanding aerosol based emissions in a Post Combustion $CO_2$ Capture process: Parameter testing and mechanisms. *International Journal of Greenhouse Gas Control.* **34**, pp. 63-74.

Majeed, H., Knuutila, H.K., Hillestad, M. and Svendsen, H.F., 2017a. Characterization and modelling of aerosol droplet in absorption columns. *International Journal of Greenhouse Gas Control.* **58**, pp. 114–126.

Majeed, H., Knuutila, H., Hillestad, M. and Svendsen. H. F. 2017b. Gas phase amine depletion created by aerosol formation and growth. *International Journal of Greenhouse Gas Control.* **64**, pp. 212-222.

Mertens, J., Knudsen, J., Thielens, M.-L. and Andersen, J. 2012. On-line monitoring and controlling emissions in amine post combustion carbon capture: A field test. *International Journal of Greenhouse Gas Control.* **6**, pp. 2–11.

Mertens, J., Brachert, L., Desagher, D., Thielens, M. L., Khakharia, P., Goetheer, E. and Schaber, K. 2014. ELPI$^+$ measurements of aerosol growth in an amine absorption column. *International Journal of Greenhouse Gas Control.* **23**, pp. 44-50.

Nguyen, T., Hilliard, M. and Rochelle, G.T. 2010. Amine volatility in $CO_2$ capture. *International Journal of Greenhouse Gas Control*. **4**, pp. 707–715.

Parliament of Australia. 2010. *Human contribution to climate change*. Available from: https://www.aph.gov.au/About_Parliament/Parliamentary_Departments/Parliamentary_Library/Browse_by_Topic/ClimateChangeold/whyClimate/human/human

Rao, A. B. and Rubin, E. S. 2002. A technical, economic and environmental assessment of amine-based $CO_2$ capture technology for power plant greenhouse gas control. *Environmental Science and Technology*. **36** (20), pp. 4467-4475.

Rochelle, G. T. 2009. Amine Scrubbing for $CO_2$ Capture. *Science*. **325**, pp. 1652-1654.

Rousseau, R.W. 1987. *Handbook of Separation Process Technology*.

Schaber, K. 1994. Aerosol formation in absorption processes. *Chemical Engineering Science*. **50**, pp. 1347–1360.

Seader, J.D., Henley, E.J. and Roper, D.K., 1998. *Separation process principles*.

Seinfield, J.H.P., Spyros N, *Atmospheric Chemistry and Physics: From Air Pollution to Climate Change*. Third ed2016, New Jersey: John Wiley and Sons, Inc. 449.

Sosso, G.C., et al., *Crystal Nucleation in Liquids: Open Questions and Future Challenges in Molecular Dynamics Simulations.* Chemical Reviews, 2016. **116**(12): p. 7078-7116.

Trollebø, A.A., Saeed, M., Hartono, A., Kim, I. and Svendsen, H.F. 2013. Vapour-Liquid Equilibrium for Novel Solvents for $CO_2$ Post Combustion Capture. *Energy Procedia*. **37**, pp. 2066–2075.

Yasuoka, K. and M. Matsumoto, *Molecular dynamics of homogeneous nucleation in the vapor phase. I. Lennard-Jones fluid.* The Journal of Chemical Physics, 1998a. **109**(19): p. 8451-8462.

Yasuoka, K. and M. Matsumoto, *Molecular dynamics of homogeneous nucleation in the vapor phase. II. Water*. The Journal of Chemical Physics, 1998b. **109**(19): p. 8463-8470.

# Appendix A. Parameters for kinetic reactions

| Reaction | k | E (cal/mol) | Reaction rate, r |
|---|---|---|---|
| $CO_2 + OH^- \rightarrow HCO_3^-$ | $4.32 \times 10^{13}$ | 13249 | $[CO_2][OH^-]$ |
| $HCO_3^- \rightarrow CO_2 + OH^-$ | $2.38 \times 10^{17}$ | 29451 | $[HCO_3^-]$ |
| $MEA + CO_2 + H_2O \rightarrow MEACOO^- + H_3O^+$ | $9.77 \times 10^{10}$ | 9855.8 | $[MEA][CO_2]$ |
| $MEACOO^- + H_3O^+ \rightarrow MEA + CO_2 + H_2O$ | $3.23 \times 10^{19}$ | 15655 | $[MEACOO^-][H_3O^+]$ |